Aalborg University

Chemical Engineering

Master thesis

Novel BDT-difluorophenyl polymers for organic photovoltaics

Authors:
Christian Linnebjerg Lausen
Morten Mortensen

Supervisors:
Zhengkun Du
Donghong Yu

AALBORG UNIVERSITY
DENMARK

May 30, 2016

AALBORG UNIVERSITY
DENMARK

Department of Biotechnology, Chemistry and Environmental Engineering
Frederik Bajers Vej 7H, 9220 Aalborg Øst
Telephone (+45) 99 40 84 90
www.en.bio.aau.dk

Title:
Novel BDT-difluorophenyl polymers for organic photovoltaics

Theme:
Polymer technology

Project period:
September 1^{st} 2015 to May 30^{th} 2016

Project group: 1.306 E15-F16

Participants:
Christian Linnebjerg Lausen

Morten Mortensen

Supervisors
Zhengkun Du
Donghong Yu

Pages: 52 (65 with appendix)

Appendices: 2

Finished May 30^{th} 2016

Abstract:

This project aimed to synthesize a novel BDT-based donor-acceptor (D-A) copolymer containing difluorophenyl, and to make organic photovoltaic devices and characterise these. The highest PCE obtained was 8%. CV, UV-VIS and AFM was performed to study the characteristics of the devices more in depth. In addition to the novel polymer, four polymers were synthesised based on two acceptors and two donors, the donors having either furan or thiophene branching out from the BDT backbone. These were used for devices to study the impact of exchanging oxygen for sulphur in the aromatic system of the polymer. The thiophene containing polymer proved to outperform the furan containing polymer.

AALBORG UNIVERSITY
DENMARK

Department of Biotechnology, Chemistry and Environmental Engineering
Frederik Bajers Vej 7H, 9220 Aalborg Øst
Telefon (+45) 99 40 84 90
www.bio.aau.dk

Titel:
Nyskabende BDT-Difluorophenyl baseret polymer til brug i organiske solceller

Tema:
Polymer Teknologi

Projekt periode:
1. September 2015 til 30. Maj 2016

Projekt Gruppe: 1.306 E15-F16

Deltagere:
Christian Linnebjerg Lausen

Morten Mortensen

Vejledere
Zhengkun Du
Donghong Yu

Sider: 52 (65 med appendiks)

Appendiks: 2

Færdiggjort 30. Maj 2016

Synopsis:

Dette projekts mål var at syntesisere en nytænkt BDT-baseret donor-acceptor (D-A) copolymer som indeholder difluorophenyl og så at fremstille organiske fotovoltaiske celler for så at karakterisere deres egenskaber. Den celle der havde højest effektivitet formåede at levere 8% PCE. Cyklisk voltammetri, UV-Vis og AFM blev brugt til at undersøge karakteristikkerne på de mest interessante solceller. Udover den nytænkte fluor indholdende polymer, så blev der polymeriseret 4 polymerer, ud fra kendte monomerer. Disse var 2 donorer, med furan eller thiophen ringe bundet til BDT rygraden, og de 2 acceptorer er velkendte og nemt tilgængelige. Disse 4 polymerer blev syntetiseret for at undersøge indvirkningen af at den eneste forskel mellem 2 polymerer er om det er et svovl eller et oxygen atom der sidder forgrenet ud fra rygraden. Den svovlholdige polymer viste sig at være væsentlig bedre end den oxygenholdige modpart.

Preface

This Master thesis is composed by Christian Linnebjerg Lavsen and Morten Mortensen during the 9th and 10th semester of Chemical Engineering at Aalborg University.

Initially this project was supposed to complete a BDT based polymer with a single fluorine on each phenyl ring, with the fluorine placed in para position facing down towards the BDT backbone. The primary motivation for this, was that donor moiety has not been tested before, giving a sort of competitive feeling of doing something new. Due to fluorines properties in organic photovoltaics, it is very popular to introduce into existing polymers, which meant that we also had to compete with time until another research group would synthesize and test this donor moiety.

While we used the first period of time polymerizing BDT furan and thiophene polymers, as soon as they had been shipped for production in Qingdao, China, we started working towards the single fluorine phenyl BDT donor. During the coupling of the phenyl rings to BDT, our secondary supervisor approached us. He had been contacted by a friend in China who had spotted "our" donor in a very newly published paper.

Therefore, after consulting our supervisors, we set out to produce a donor moiety with two fluorine atoms on each phenyl ring, both in meta position. Recently a few papers have been published containing two fluorine atoms on both the donor and the acceptor moiety, so it was decided to produce a new donor with four fluorine atoms, which is the final product of this report.

The group would like to thank supervisors Zhengkun Du and Donghong Yu. We would also like to thank Professor Renqiang Yang at Qingdao Institute of Bioenergy and Bioprocess Technology(QIBEBT) for inviting us to use the facilities there for our device processing. In addition, we want to thank Junyi Wang, Linrui Duan, Zurong Du and Yongchao Zhang for their aid in making the OPV devices and general help during our stay in Qingdao, China. We would further like to thank Kacper Januchta for assistance with AFM measurements. Lastly we would like to thank Joseph Iruthayaraj and his PhD student Jakob Ege Friis for assistance with cyclic voltammetry at Århus University.

Reading Instruction

Citations in this report are referred to as [Author, Year of release]. Please note that when a citation is unpublished, a year of release will not be mentioned, but referred to as [Author].

In the bibliography the sources are listed in the order of first occurrence, and will be referred to as:

Articles:
Author. Title. *Journal*, Volume(Number):Pages, Year of release. ISSN. DOI. Page reference

Books:
Author. *Title*. Publisher, Year of release. ISBN. Page reference

Unpublished work:
Author. Title. URL Link. Page reference

Appendices

The appendices can be found on the included CD on the back cover of the report. A list of appendices is as follows:

Appendix A - NMR data (in the back of the report)
Appendix B - Experimental data (as datafile)

Contents

1 | Introduction

Global demand for energy is rising, in 2008 16.5 TW was consumed worldwide, and this number is expected to keep rising[Larsen-Olsen *et al.*, 2011]. Most of the energy consumed is in the form of fossil fuels, which are consumed at a rate too fast for the natural deposits to regenerate[BP, 2014]. The fossil fuels are also a cause of environmental damage and climate change.

The past decades have seen advancements in several sustainable forms of energy, biomass, wave, wind, waterflow, fusion energy and solar power. While fusion alone could potentially power the entire world, the technology is still in its infancy and will require several decades before it becomes useful[Ward, 2008]. Meanwhile, the other technologies are already being used to various extent, but have not been able to become as cost efficient or stable as the fossil fuels. Biomass is made from crops, taking up arable land that could otherwise be used to feed the growing global population and wind energy is too inconsistent as power is provided based on the fickle weather patterns. Solar power has the potential to cover the entire worlds energy consumption. The sun emits a tremendous amount of energy at all times and 1.2×10^5 TW reaches the Earth, more than enough to cover the needs of the entire world[Larsen-Olsen *et al.*, 2011]. Collecting, storing and distributing this energy, however, has several issues.

Devices for collecting solar energy have existed since the 1940s in the form of inorganic silica based solar cells (ISC), although at this time the efficiency was less than 1% [Miles *et al.*, 2007]. The technology continued to improve leading to commercial solar cells with a Power Conversion Efficiency(PCE) above 20% [Larsen-Olsen *et al.*, 2011]. Using these the world energy consumption could be met, however, since inorganic solar cells are made from silica wafers, the production of the inorganic solar cells requires energy demanding and expensive material processing, leading to a long energy payback time[Miles *et al.*, 2007]. In order to make solar cells with lower energy payback time other technologies are being developed, such as dye-sensitized solar cells and organic solar cells, both of which are so-called thin film solar cells.

Organic solar cells are made from organic materials. There are several different types of organic solarcells, but one of the most promising types is Bulk Heterojunction(BHJ) solar cells. BHJ solar cells consists of an electron donor material(DONOR), for example a conjugated polymer, and an acceptor moiety(ACCEPTOR), usually a fullerene derivative($PC_{61}BM$ for instance), mixed before the device is processed. This has the advantage of maximising the interfacial area between DONOR and ACCEPTOR, minimizing exciton travel time and facilitates charge collection at the electrodes[Zhou

et al., 2012]. In order to maximise the PCE of organic photovoltaics(OPVs), several factors can be improved upon, the general formula for calculating PCE is:

$$PCE = \frac{V_{OC} * J_{SC} * FF}{P_{in}} \tag{1.1}$$

In which V_{OC} is the open circuit voltage, J_{SC} is the short circuit current, FF is the fill factor and P_{in} is the total solar power that hits the cell. V_{OC} can be altered by tuning the HOMO level of the Donor material as it is correlated to the difference between the HOMO level of the donor and the LUMO level of the acceptor. A lower HOMO level generally yields a higher V_{OC}, however, a minimum difference of 0.3eV between the LUMO levels of the DONOR and the ACCEPTOR is necessary for exciton splitting and charge dissociation to be effective[Zhou *et al.*, 2012]. J_{SC} is based on the number of excitons created by sun light hitting the device. A higher J_{SC} can be obtained by increasing the ability of the active layer to absorb light and create excitons. Since most of the sunlight is in the 380 to 900 nm range the donor material should have broad absorption in this area. This requires a narrow bandgap, which is the difference between HOMO and LUMO level of the material[Zhou *et al.*, 2012]. FF is reliant on the morphology of the active layer which should be optimized for charge separation and charge transport[Zhou *et al.*, 2012].

For OPVs an effective approach has been using Donor-Acceptor(D-A) copolymers as electron donor. These polymers have a backbone consisting of an electron-rich donor and an electron deficient acceptor moiety. This setup allows for internal charge transfer from the donor to the acceptor, leading to a low bandgap, which facilitates a high J_{SC}. The structure also allows the conjugated backbone to be more planar, facilitating the π-electron delocalisation[Zhou *et al.*, 2012]. Using D-A copolymers also gives the advantage of being able to tune either of the monomers to improve performance.

The photovoltaic devices made in the main part of this project will consist of a D-A co-polymer with a donor moiety of benzo[1,2-b:4,5-b']dithiophene (BDT) substituted with two difluoroalkoxyphenyl molecules on the central benzene ring. BDT is chosen as a backbone due to its planar structure, easy substitution, good electron transporting properties and ease of processability[Zhou *et al.*, 2012]. Fluorine is added to the backbone because it has been shown to lower both HOMO and LUMO level of the polymer while not changing the bandgap[Zhou *et al.*, 2011]. This primarily affects the V_{OC} as the HOMO level is lowered.

1.1 Problem statement

The purpose of the project is to synthesize a donor monomer containing flourine, polymerise it with the acceptors DTBT and DPP, and use the resulting polymers in the active layer of photovoltaic devices. Both the polymers and the devices will be tested and characterized.

A secondary part of the project will be synthesizing and making devices on four polymers made from two acceptors and two donors. The donors only difference is that the 5 membered ring branching from the BDT, is either a furan or a thiophene, to study the impact of a single atom changing from oxygen to sulphur.

2 | Theory

2.1 Device Theory

In order to obtain as much power from the sunlight as possible, OPV devices have a planar layered structure on a glass substrate.

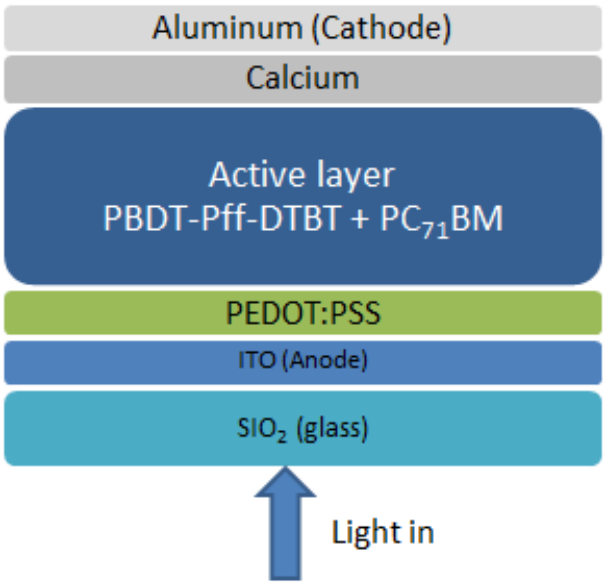

Figure 2.1: The layer structure of OPV devices.

The bottom layer is a transparent Indium-tin-oxide(ITO) which acts as the high-workfunction electrode(anode)[Spanggaard & Krebs, 2004]. Since there are large variations between in the ITO from different manufacturers and batches, it can be hard to control the morphology of the ITO, however, acid etching and ozone cleaning have been shown to minimise the differences[Spanggaard & Krebs, 2004]. ITO also has the issue that it can interact with the active layer if it is in direct contact. Both oxygen and indium was found to diffuse into the active layer at the interface between the active layer and the electrode[Schlatmann *et al.*, 1996][Scott *et al.*, 1996].

To avoid this, a layer of poly-(3,4-ethylenedioxytiophene) with polystyrene sulfonic acid(PEDOT:PSS) is coated on top of the ITO. This also serves as a hole-transporting layer in order to facilitate fast charge separation and avoid recombination of the electron and hole[Kirchmeyer & Reuter, 2005][Spanggaard & Krebs, 2004]. A thin PEDOT:PSS film also serves to make a smoother surface compared to ITO[Kirchmeyer & Reuter,

2005][Spanggaard & Krebs, 2004].

The third layer is the active layer, in which the DONOR polymer and ACCEPTOR fullerene in BHJ is coated on top of the PEDOT:PSS. This is where most OPVs differ since the possible combinations of small molecules or polymers as donors and fullerene derivatives as acceptors are almost endless. The active layer is where the photovoltaic effect in OPVs originate. The DONOR absorbs sunlight in the 450-700nm range (visible light). The energy absorbed excites electrons in the HOMO(valence band) of the DONOR, causing them to move to the LUMO(conductive band) of the DONOR leaving behind an electron hole. The excited electron and the electron hole are collectively called an exciton. The hole and the excited electron then have to be split which happens by making sure the LUMO level of the ACCEPTOR is slightly lower to that of the DONOR, around 0.3 eV to ensure efficient charge separation. Once separated the electron should move on towards the cathode, while the hole moves towards the anode. A good BHJ and morphology are both important factors for the charge transport[Zhou *et al.*, 2012].

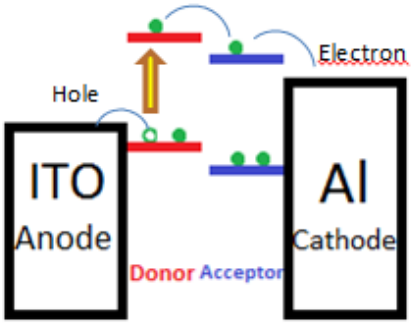

Figure 2.2: Charge formation and transfer in OPVs, inspired by [Savenije, n.d.]

The External Quantum Efficiency(EQE) of the device is the amount of electrons excited per photon that hits the device. EQE is measured over a range of different wavelengths by hitting the device with monochromatic light at the different wavelengths and measuring. The total EQE of an OPV device can be obtained by integrating over the entire electromagnetic range of sunlight. This value can be used to evaluate how efficiently the OPV converts energy from incoming photons[Secaites *et al.*, 2009]. Calculating J_{SC} from EQE is done using Equation 2.1.

$$J_{SC} = A_{cell}^{-1} \times \int_{\lambda=0}^{\lambda=\lambda_g} \phi_p(\lambda)\eta_{EQE}(\lambda)d\lambda \tag{2.1}$$

A_{cell} is the cell area of the device, λ is the wavelength of the light, λ_g is the largest wavelength absorbed by the DONOR, $\phi_p(\lambda)$ is the photon flux and $\eta_{EQE}(\lambda)$ is the EQE limit for each wavelength[Secaites *et al.*, 2009].

For the DONOR part of the BHJ, the important attributes are the ability to absorb energy from sunlight and use this energy to create excitons, as well as the ability to split the electron and the hole. For the ACCEPTOR, the most important factor is the ability to accept the excited electrons from the DONOR and transport these to the cathode.

The fourth and final layer is the low-workfunction electrode (cathode), made from an electropositive metal such as Al[Spanggaard & Krebs, 2004]. However, interactions

between the cathode and the active layer cause the formation of an insulating layer decreasing efficiency. To avoid this an additional layer is added between the cathode and the active layer, this secondary layer can for instance be LiF, MgO or Ca[Spanggaard & Krebs, 2004].

2.2 Syntheses

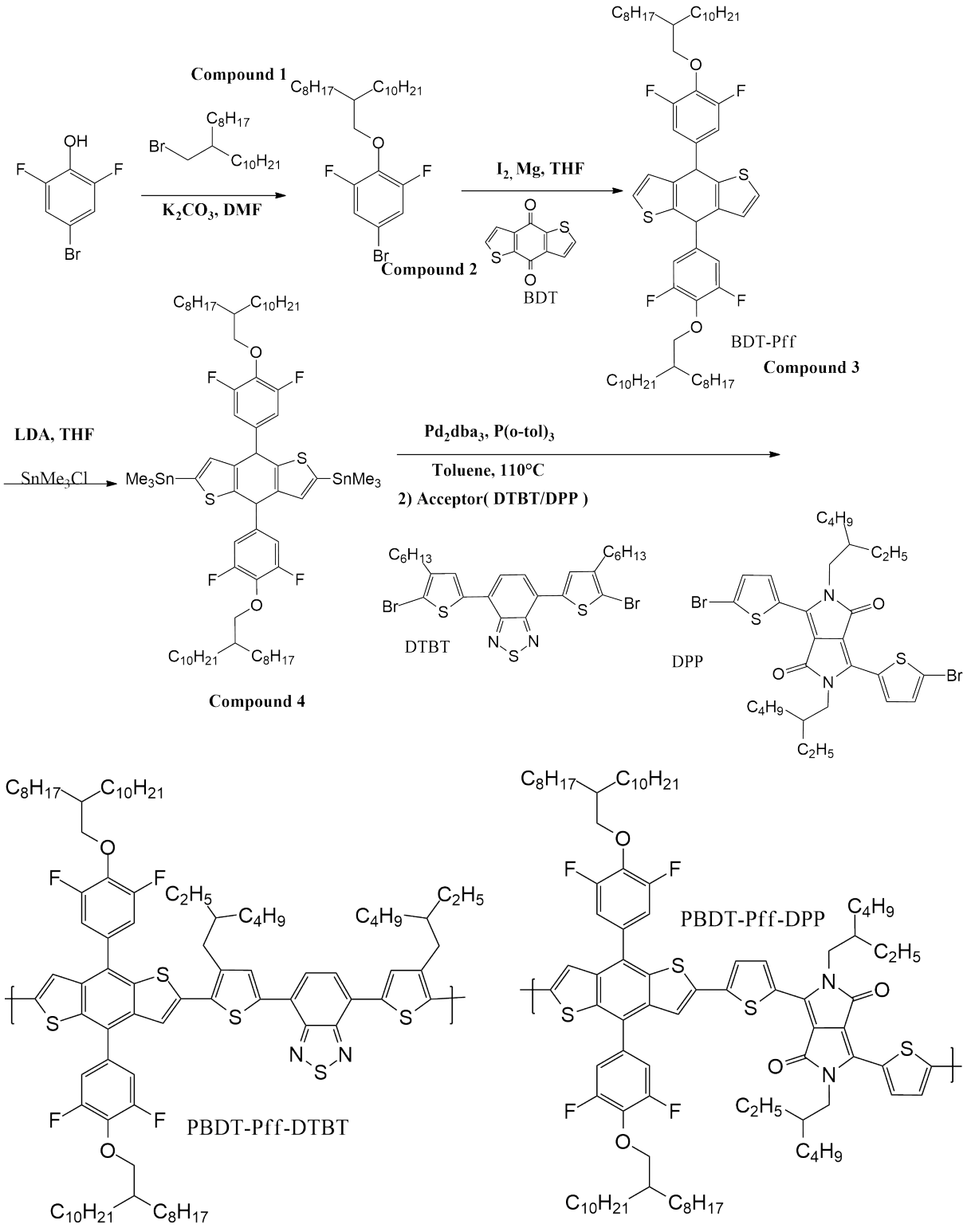

Figure 2.3: Full synthesis route for PBDT-Pff-DPP and PBDT-Pff-DTBT.

2.2.1 Bromination of 2-octyl-1-dodecanol

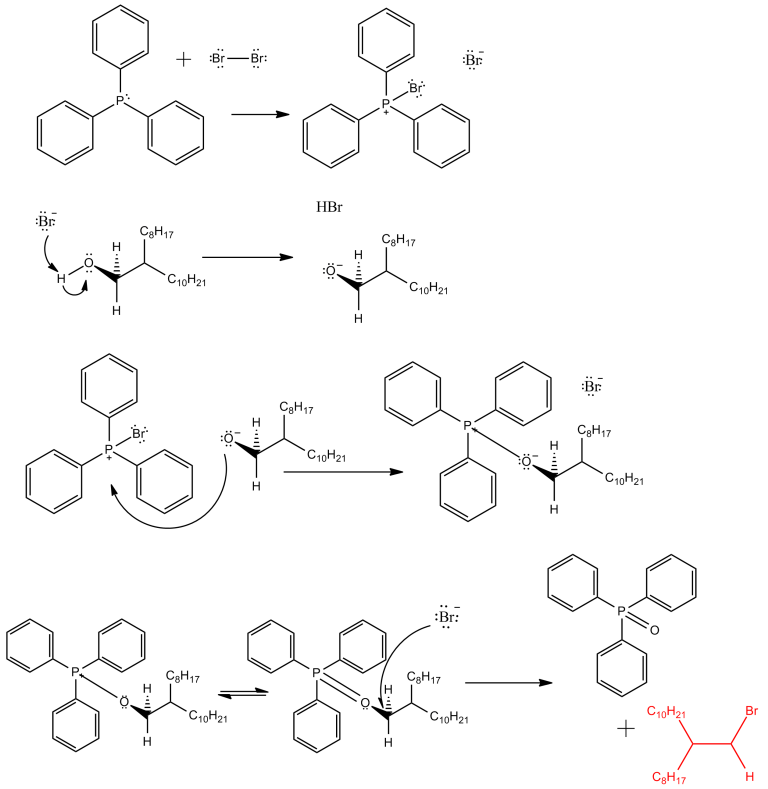

Figure 2.4: Bromination of 2-octyl-1-dodecanol

The first step in the synthesis of BDT-Pff-DTBT and BDT-Pff-DPP is to brominate the 2-octyl-1-dodecanol using an Appel nucleophile substitution reaction. In this reaction triphenylphosphine(PPh_3) is halogenated by Br^2, leaving a free Br^- to react with 2-octyl-1-dodecanol to form HBr as well as an alkoxide.

This alkoxide attacks the halogenated PPh_3, causing it to release Br^- which then attacks the carbon stereocenter in an SN_2 reaction which causes the product 2-octyl-1-dodecanyl bromide to have inverted sterochemistry. The formation of a strong P=O double bond in the PPh_3 is the driving force in the reaction, this byproduct is called triphenylphosphine oxide.

2.2.2 Synthesis of BDT-Pff

The BDT-Pff monomer is synthesised in four steps. The first three steps are to synthesise the monomer while the last step is to add trimethyltin in order to prepare it for polymerization by Stille coupling.

The first step is a condensation reaction in which 2-octyl-1-dodecanyl bromide and 4-bromo-2,6-difluorophenol react to form 1-bromo-3,5-difluoro-4-(icosyloxy)benzene, also releasing HBr which reacts with K_2CO_3 to form KBr.

Step two is to prepare 1-bromo-3,5-difluoro-4-(icosyloxy)benzene as a Grignard reagent by reaction with Mg in THF.

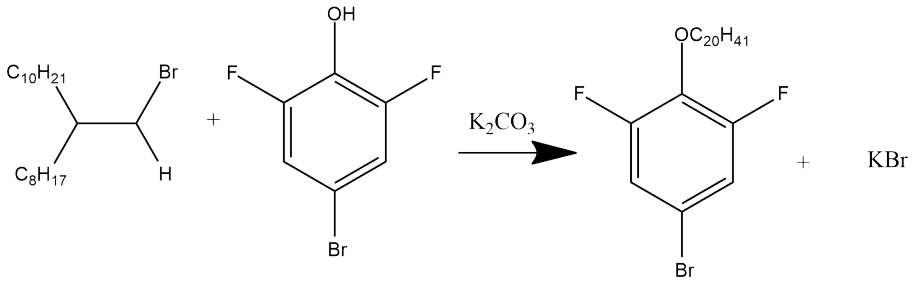

Figure 2.5: Synthesis of 1-bromo-3,5-difluoro-4-(icosyloxy)benzene in a condensation reaction.

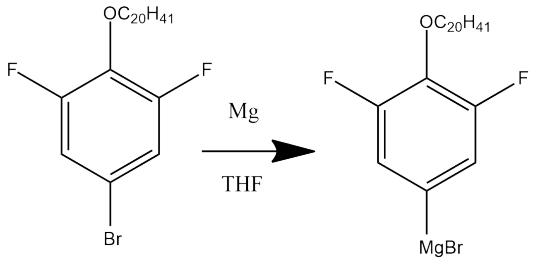

Figure 2.6: 1-bromo-3,5-difluoro-4-(icosyloxy)benzene is used to make a Grignard reagent.

The Grignard reagent is then instantly used in step three which is a nucleophile addition in which the nucleophile is the carbanion from the Grignard reagent[McMurry, 2011]. In order to remove the hydroxyl groups a solution of HCl in water with $SnCl_2$ is added. The HCl donates a proton to the hydroxyl groups making OH_2^+ groups, which is a good leaving group. The OH_2^+ groups then each take an electron from the aromatic structure of the BDT-Pff. This electron deficit is then corrected taking electrons from the free Cl^- from the HCl solution, oxidising $SnCl_2$ from Sn(II) to Sn(IV) to yield $SnCl_4$.

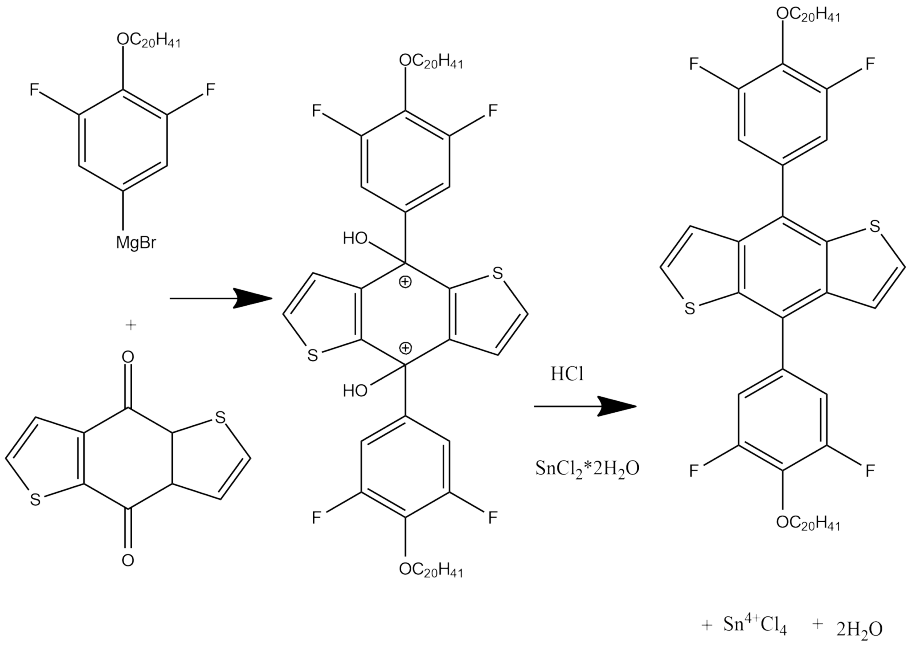

Figure 2.7: Reaction to yield BDT-Pff using $SnCl_2$ in aqueous HCl.

The fourth step is a stannylation using Lithium Diisopropylamide(LDA) Diisopropylamide is treated with n-BuLi replacing a hydrogen atom with Lithium to yield LDA, which is then immediately used in the further reaction to deprotonate the BDT-Pff allowing $SnMe_3Cl$ to react. This reaction yields the stannylated BDT-Pff monomer as well as LiCl and Diisopropylamide.

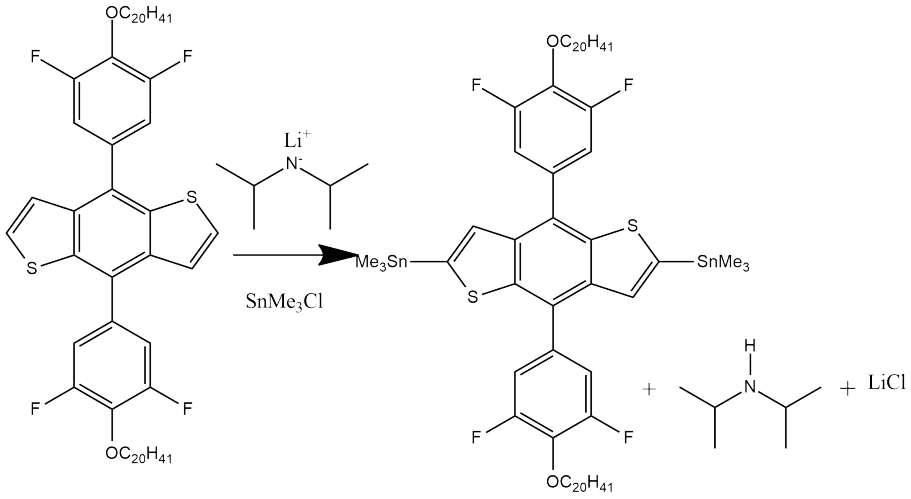

Figure 2.8: Stannylation of BDT-Pff to prepare for Stille coupling.

2.2.3 Acceptor monomers

The synthesis of the acceptor molecule DTBT is done in two steps. The first step is a Suzuki coupling reaction to make the monomer, and the second is an NBS bromination to prepare it for a Stille coupling reaction with the donor monomer.

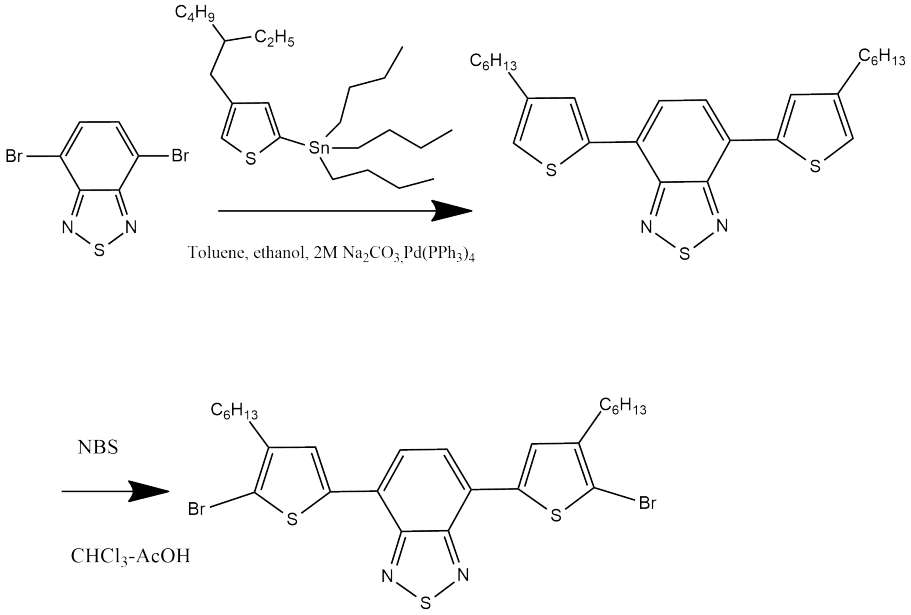

Figure 2.9: Synthesis and bromination of DTBT monomer

The other acceptor molecule 1,4-Diketopyrollo[3,4-c]pyrole(DPP) was bought complete and brominated to prepare it for coupling with the donor monomer.

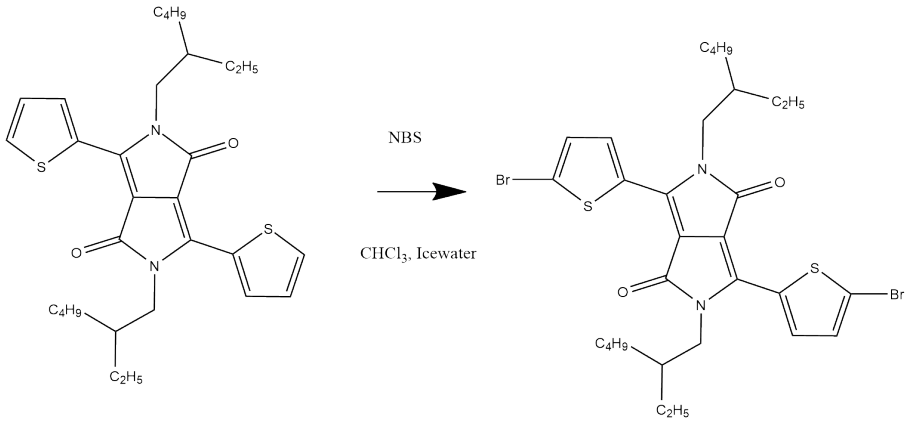

Figure 2.10: Bromination of DPP monomer

2.2.4 Polymerisation of BDT-Pff with DTBT and DPP

The polymerisation is done by Stille coupling. An organic halide reacts with a palladium(0) complex to form an organopalladium halide intermediate which undergoes transmetalation. Finally, a reductive elimination restores the palladium(0) complex and yields the final product[Bao *et al.*, 1995]. This reaction is done with both DTBT and DPP yielding PBDT-Pff-DTBT and PBDT-Pff-DPP respectively.

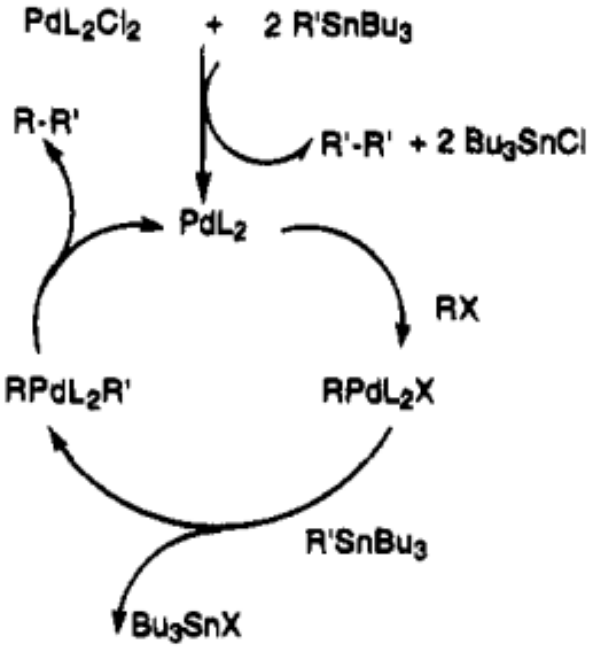

Figure 2.11: Stille coupling reaction mechanism as proposed by Bao *et al.* [1995].

2.3 Thiophene and furan derivatives

Aside from the production of the novel polymers described above, this project also studies the difference in performance of photovoltaics between two otherwise similar BDT based

polymers containing furan and thiophene groups respectively. The only difference is, thus, that an oxygen atom is exchanged with a sulphur atom.

Both thiophenes and furans are aromatic due to one of their lone pairs being delocalised into the ring. The other lone pair is in the same plane as the ring system. There is, however, a difference between the properties of the two different ring systems, since the electron density is different between the two. Oxygen has a higher electronegativity than sulphur(3.4 compared to 2.6) which means the electron density in the aromatic system should be lower for the furan. However, since the oxygen is also better at delocalising its lone pair into the aromatic system compared to sulphur, thiophene actually has less electron density in the aromatic system. The ability to delocalise the lone pair mirrors the basicity of the protonated form of the compounds with protonated furan having a pKa of -2.1 and protonated thiophene having a pKa of -4.5[Spivey, 20112]. A lower electron density in the aromatic system in a photovoltaic polymer has been linked to a deeper HOMO level which can lead to a better V_{OC}. [Zhou *et al.*, 2011]

Aside from the difference in electron properties between the two, there is also a slight difference in size and molecular weight of the molecules as sulphur is larger and heavier than oxygen.

2.3.1 Polymerisation of BDT-TS and BDT-FS polymers

Both BDT-TS and BDT-FS are polymerised using Stille coupling as described above in 2.2.4. Both monomers are polymerised with TPD as well as PTPD making four different co-polymers.

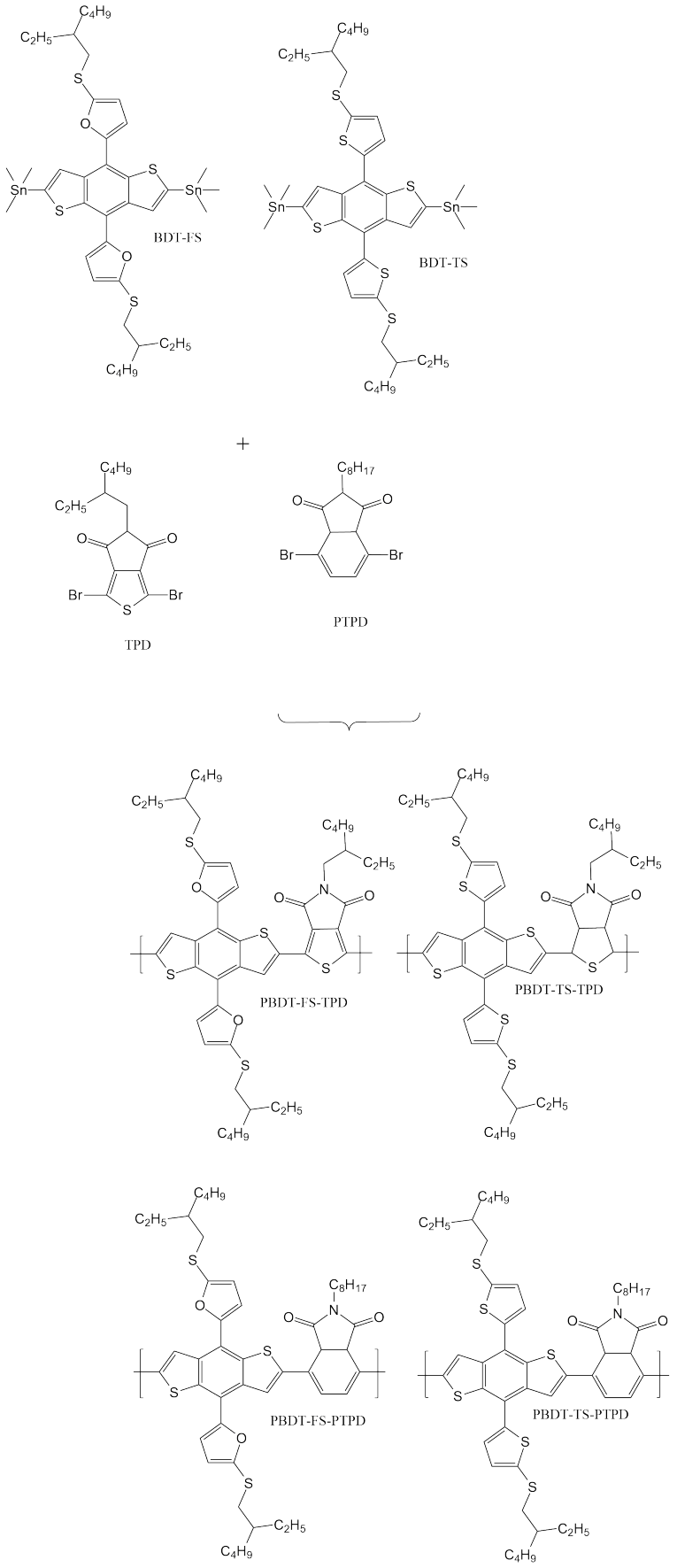

Figure 2.12: Combinations of monomers: BDT-FS, BDT-TS, TPD and PTPD, BDT-FS and BDT-TS made by Zhengkun Du, TPD and PTPD made by Wei Yue.

3 | Experimental

The initial plan for the project was to synthesize a novel Donor-Acceptor(D-A) polymer for use in organic photovoltaics. The planned donor moiety was based on a somewhat similar monomer utilizing flourine substituted benzene on a BDT backbone [Chen *et al.*, 2015]. The decision to add two flourine atoms to each benzene was based on the encouraging results from having one meta-position fluorine atom. BDT was used as a backbone since it is a common choice for D-A polymer backbones due to its structure which allows easy alkylation of the central benzene ring, while the thiophenes on either side of it provides little steric hindrance with the acceptor unit which leads to a more planar backbone for the polymer, which improves the π-delocalization[Zhou *et al.*, 2012].

The solar devices will be fabricated during a four week stay at the Qingdao Institute of Bioenergy and Bioprocess Technology(QIBEBT) in Qindao, Shandong Province, China. QIBEBT has the required instruments for processing spincoated organic solar cells, as well as many years of experience with the process. The fabrication of the photovoltaic devices will be an optimization process in which the first batch of 16 devices will consist of four columns, each having different spin speeds. The first batch is made using some different blend ratios, spin speed and different additives, thus, there are atleast 2 equal samples that only differ in a single condition, which can give understanding towards optimal conditions. After the first batch is tested the variables that prove to be beneficial to the device performance will be used in further optimization of the devices.

Aside from the novel solar cells, the project will also have a secondary goal. Studying the influence of thiophenes compared to furans on the performance of solar cells. This part of the project will consist of synthesizing one thiophene substituted monomer and one furane substituted monomer that are otherwise identical, making D-A polymers from the monomers and study the effect on the device performance while only changing from furan to thiophene, thus the only difference is eiher 2 oxygen atoms or 2 sulphur atoms in the repeating unit of each polymer.

4 | Materials and Methods

The reaction routes for the polymers are portrayed in Figure 2.3.

4.1 Synthesis of 2-octyl-1-dodecanyl bromide (Compound 1)

100 mL dichloromethane and triphenylphosphine(68 mmol, 17.84 g) was mixed at room temperature. Bromine (68 mmol, 3.484 mL) was added to a dropping funnel, dichloromethane was added as a lid, the bromine was added slowly over 45 minutes. 2-octyl-1-dodecanol (68 mmol, 20.3 g, 24.22 mL at 0.838 $\frac{g}{cm^3}$)was added to the funnel after finished addition of bromine and was added dropwise over 30 min. The reaction was left overnight. Dichloromethane was evaporated in distillation. The concentrate was washed 4 times with 50 mL pentane and the liquid filtered through a funnel with a cotton plug. The filtrate was concentrated via rotary evaporation and the product was collected as a colorless oil[He *et al.*, 2011]. 26.833 g of product was obtained. ^{1}H NMR(600MHz, $CDCl_3$), δ (ppm): 7.26 (s,1H), 3.44 (d, 2H), 1.57-1.61(m,1H), 1.53(s, 1H), 1.27-1.39(m, 32H), 0.87-0.90 (m, 6H). NMR data can be found in Section A.1.

4.2 Synthesis of 1-bromo-3,5-difluoro-4-(2-octyldodecyl)benzene (Compound 2)

9.01 g(24.9 mmol) of compound 1 was weighed off, together with 5.66 g(27 mmol) 4-bromo-2,6-difluorophenol and 12.164g(55 mmol) potassium carbonate was added into 50 mL Dimethylformamide. The reaction was stirred for 24 hours at 100°C with recondensation. After cooling to room temperature, ethyl acetate was added to the solution and the inorganic salts were filtered with vacuum filtration. The remaining salts and bottle were washed several times with ethyl acetate. The filtrate was added 50 mL ethyl acetate and 125 mL water and poured into a separation funnel. The funnel was shaken and allowed to settle until a distinct separation had occurred, with a yellow layer on top. 10.56 g(21.6 mmol) was obtained with a yield of 87%. ^{1}H NMR(600MHz, $CDCl_3$), δ (ppm): 7.26 (s, 1H), 7.08-7.05 (t, 2H), 3.99-3.98 (d,2H), 1.72-1.70(t,1H), 1.56 (s, 1H), 1.47-1.27 (m, 33H), 0.89-0.87 (t, 6H). NMR data can be found in Section A.2.

4.3 Synthesis of 4,8-bis(3,5-difluoro-4-((2-octyldodecyl)oxy)phenyl)benzo[1,2-b:4,5-b']dithiophene(compound 3)

0.5784g (23.46mmol) Mg and one particle of I is added to a flask and purged 2 times for 5min each, flushing with nitrogen between vacuum purges. 5mL THF is added to the flask containing Mg and I, 25mL is added to another flask containing 10.005g (20.4mmol) of compound 2. Under heavy stirring 10% of the compound 2 mixture is added to the reaction flask. After addition, the reaction is heated to $45°C$ for 4h and cooled to room temperature. BDT is added to a flask and purged for 3 times 5 minutes with nitrogen flush between vacuum purges. The first solution is added to the BDT system, and a $SnCl_2$ solution is made from 28mL 10% HCl in water added to 12.6362g (56mmol) $SnCl_2 \cdot *2H_2O$. The $SnCl_2$ solution is added dropwise and a distinct colorchange took place (brown to yellow). The reaction is heated slowly to $50°C$ and left for 2h. The heating is stopped and the reaction is left stirring over night. 200mL DI water is poured into the solution and the water phase was washed 3 times with hexane. After combining the organic phases, anhydrous sodium sulphate is added. The crude product is purified on a silica gel column eluting with hexane. 4.51 g (4.47 mmol) of product. Yield = 21.94%. ^{1}H NMR(600MHz, $CDCl_3$), δ (ppm): 7.45-7.46 (d, 2H), 7.32-7.33 (d, 2H), 7.26 (s, 1H), 7.25-7.23 (d, 4H), 4.15 (d, 4H), 1.83-1.80 (dd, 2H), 1.58-1.53 (m, 7H), 1.44-1.26 (m, 60H), 0.90-0.87 (m, 12H). ^{13}C NMR (150 MHz, $CDCl_3$), δ (ppm): 157.04, 156.99, 155.38, 155.38, 138.06, 136.22, 136.13, 136.04, 135.95, 133.40, 133.34, 128.47, 128.01, 122.48, 113.42, 113.39, 133.31, 133.27, 77.00, 38.92, 31.94, 31.00, 30.05, 29.67, 29.37, 26.80, 22.71, 14.14. NMR data can be found in Section A.3

4.4 Synthesis of compound 4

Argon atmosphere: 2.015g(2mmol) compound 3 was dissolved in 50 mL dry THF, and 0.85mL(6mmol) LDA is added dropwise at -40°C and stirred for 1.5h, the solution is cooled to -78°C and added to the 6.7mL trimethyltin chloride solution (in n-hexane). The solution is slowly warmed to room temp and allowed to stir overnight. The reaction is quenched with DI water and extracted three times with diethyl ether. The combined organic phase is dried over magnesium sulphate. After removing of solvents, the crude product is recrystallized from acetone. 1.8 g(1.35 mmol) product obtained, giving a yield of 67.5%. ^{1}H NMR(600MHz, $CDCl_3$), δ (ppm): 7.33 (m, 2H), 7.27 (m, 2H), 7.26 (s, 1H), 7.25 (m, 2H), 4.17 (d, 4H), 1.86-1.82 (m, 2H), 1.59-1.55 (m, 4H) 1.48-1.29(m, 61H), 0.91-0.88 (m, 12H), 0.45-0.35 (t, 18H). ^{13}C NMR (150 MHz, $CDCl_3$), δ (ppm): 157.04, 156.99, 155.39, 155.34, 143.25, 142.34, 136.78, 135.98. 135.89, 135.79, 134.23, 134.17, 134.11, 129.98, 126.84, 113.49, 113.45, 113.37, 113.34, 77.00, 38.96, 31.95, 31.05, 30.08, 29.72, 29.68, 29.64, 29.39, 29.38, 26.83, 22.72, 14.15. NMR data can be found in Section A.4

4.5 Co-polymerization of BDT-Pff and DTBT

0.2666g(0.2mmol) Compound 4 and 0.1365g(0.2mmol) DTBT is dissolved in 9mL toluene in a single necked 25mL flask. 2.6mg $Pd_2\,(dba)$ and 5.2mg $p\,(o-tol)_3$ was added to the flask. The reaction is purged 5 times using vacuum and nitrogen, while the system is kept at -78°C and stirred. The mixture is heated to room temperature and slowly to 70°C , 90°C and finally kept at reflux for 2h. The product is purified on a silica gel column using chlorobenzene and further purified with soxhlet extraction using hexane, acetone and chloroform. NMR data for DTBT can be found in Section A.18.

4.6 Co-polymerization of BDT-Pff and DPP

0.2666g(0.2mmol) Compound 4 and 0.1365g(0.2mmol) DPP is dissolved in 9mL toluene in a single necked 25mL flask. 2.6mg $Pd_2\,(dba)$ and 5.2mg $p\,(o-tol)_3$ was added to the flask. The reaction is purged 5 times using vacuum and nitrogen, while the system is kept at -78°C and stirred. The mixture is heated to room temperature and slowly to 70°C , 90°C and finally kept at reflux for 2h. The product is purified on a silica gel column using chlorobenzene and further purified using soxhlet using hexane, acetone and chloroform.

4.7 Co-polymerization of BDT-TS and PTPD

0.2906g (0.3 mmol) BDT-TS and 0.1251 (0.3 mmol) TPD is dissolved 10 mL anhydrous toluene in a flask along with 7 mg (0.006 mmol) $Pd(PPh_3)_4$ and 2 mL anhydrous DMF. The reaction is purged 5 times with 10 minutes of vacuum separated by filling with nitrogen. This is done at -78°C . The reaction is slowly heated to reflux at 110°C and kept there for 24h. After the first hour a color change from yellow to red occurred. The reaction was added to methanol and polymer solidified on the bottom of the flask.Purified by flash column. NMR data for the donor and acceptor can be found in Section A.16 and Section A.21.

4.8 Co-polymerization of BDT-TS and TPD

0.2905g (0.3 mmol) BDT-TS and 0.1269 (0.3 mmol) TPD is dissolved 10 mL anhydrous toluene in a flask along with 7 mg (0.006 mmol) $Pd(PPh_3)_4$ and 2 mL anhydrous DMF. The reaction is purged 5 times with 10 minutes of vacuum separated by filling with nitrogen. This is done at -78°C . The reaction is slowly heated to reflux at 110°C and kept there for 18h. After the first hour a color change from yellow to red occurred. The reaction was added to methanol and polymer solidified on the bottom of the flask. The product is suction filtered and washed with hexane, then acetone. It is dissolved in chloroform and pushed through a silica gel packed with hexane with chloroform as eluent. NMR data for the donor and acceptor can be found in Section A.16 and Section A.19

4.9 Co-polymerization of BDT-FS and PTPD

0.2809g (0.3 mmol) BDT-TS and 0.1251 (0.3 mmol) TPD is dissolved 10 mL anhydrous toluene in a flask along with 7 mg (0.006 mmol) $Pd(PPh_3)_4$ and 2 mL anhydrous DMF.

The reaction is purged 5 times with 10 minutes of vacuum separated by filling with nitrogen. This is done at -78°C . The reaction is slowly heated to reflux at 110°C and kept there for 24h. After the first hour a color change from yellow to red occurred. The reaction was added to methanol and polymer solidified on the bottom of the flask. Purified by flash column. NMR data for the donor and acceptor can be found in Section A.16 and Section A.21

4.10 Co-polymerization of BDT-FS and TPD

0.2808g (0.3 mmol) BDT-TS and 0.1270 (0.3 mmol) TPD is dissolved 10 mL anhydrous toluene in a flask along with 7 mg (0.006 mmol) $Pd(PPh_3)_4$ and 2 mL anhydrous DMF. The reaction is purged 5 times with 10 minutes of vacuum separated by filling with nitrogen. This is done at -78°C . The reaction is slowly heated to reflux at 110°C and kept there for 24h. After the first hour a color change from yellow to red occurred. The reaction was added to methanol and polymer solidified on the bottom of the flask. The product is suction filtered and washed with hexane, then acetone. It is dissolved in chloroform and pushed through a silica gel packed with hexane with chloroform as eluent. NMR data for the donor and acceptor can be found in Section A.16 and Section A.19

4.11 Device Fabrication

4.11.1 Glass preparation

32 pieces of ITO coated substrates were put into a sample stage and placed in a beaker. Around 200 ml of concentrated cleaning solution is added to 5L DI water to produce the cleaning mix, the glass is covered in the cleaning mixture dilute and sonicated for 15 minutes. The cleaning mixture is removed and fresh DI water is poured into the beaker, and a 15 min sonication is started. The substrates are covered by acetone and sonicated for 15 minutes and another 15 minutes with fresh DI water afterwards. Last round of cleaning is 15 min sonication covered by isopropanol, the glass and isopropanol are left in the beaker, and covered with tinfoil until needed.

Each glass was blowdried with pure nitrogen, and placed in a glass petridish. The petridish was placed inside a plasmaoven, cooling, vacuum and a small inlet of oxygen was started. The samples were treated for 2 times 3 minutes with a small cooling break inbetween.

The substrates were spincoated at 4k RPM for 2 min using PEDOT:PSS from Heraeus, being careful not to touch the ITO with the syringe. The samples were covered by glass again, and put into an oven at 110°C to evaporate the water that the PEDOT:PSS could contain.

4.11.2 Solution preparation

Each solution was prepared in a 2mL vial with a stirrer inside. The general solution concentration prepared was 3µg/100µL of combined DONOR and ACCEPTER, which was dissolved in DCB. An important step was to ensure that the mixture was homogeneous and without sedimentation, and then allowing the mixture to stir for about 6 hours before

use. Additives had to be mixed for atleast 1 hour, and no longer than 4 hours, as inlab tests had shown that the effect from the additives was decreasing after the 2-3 hour span.

4.11.3 Spincoating

The PEDOT:PSS coated ITO glass was placed individually on the spincoater and 25µL of solution was carefully spread across the ITO glass, making sure to not touch the substrate, while trying to cover the entire cell with solution. Immediately after depositing the solution the spin was started, varying between 750 to 3k RPM for 1 minute. At slower RPM values, additional time could be necessary to dry the solution properly. The coated device was placed on a piece of paper to absorb the unused solution and the cell was checked for homogeneity. If major damage on the coated layer was visible, the same solution was repeated. After coating all 16 devices, they were immediately transferred to the evaporation chamber to prevent damage to the active layer.

4.11.4 Device processing

Step by step on the evaporation process of OPV devices creation. A sample stage with 16 slots are mounted in the top of the evaporation chamber. A small pellet of calcium and a prepared aluminium swirl are put in separate containers, calcium in the first electrode to the left, and aluminium in the second electrode to the right. The door to the chamber is closed and securely sealed. On the control board for the evaporator, it was ensured that everything had power, and the power button was pressed, then the mechanical pump and bypass valve was turned on. When the pressure was below 5 Pa, the bypass valve were turned off, and the forline valve, molecular pump and main valve was turned on in an interval of 5-10 seconds between the last three. The most critical information of the molecular pump is the RPM, when the RPM has reached max of 24.000, then the pressure should be below $5 \cdot 10^{-4} Pa$. When the vacuum is in place, the first electrode was powered on and the current was slowly increased until displaying a frequency decrease of about 1 hz per 2-3 seconds, once the frequency had decreased about 100 hz, the shield above electrode 1 was removed and the sample stage started rotation. After another 100 hz frequency decrease, the electrode shield was put back in place and the current over the electrode was reduced to 0. Then the power was redirected to the second electrode, and the current was slowly increased until displaying a frequency decrease of about 10 hz per sec, and the current was gradually changed to keep the frequency drop at about 10 hz per sec until the aluminium was depleted, which was indicated by no longer depositing film onto the samples. Shut-off sequence was main valve, molecular pump and wait for the RPM to hit 14000, then open the gas inlet, and wait for the molecular pump to turn off completely before opening the chamber.

5 | Results and discussion

5.1 PBDT-Pff polymer

5.1.1 Photovoltaic properties

Using the lab equipment at QIBEBTS, it was made possible to manufacture the synthesized polymer into devices, thus learning about the process and the photovoltaic properties of PBDT-Pff-DTBT. Unfortunately, it was discovered that the second synthesised polymer PBDT-Pff-DPP was insoluble in DCB, therefore it was decided to focus the work on PBDT-Pff-DTBT instead.

When a new polymer is synthesised, it is sometimes possible to obtain information from papers of similar monomers, this can be knowledge of blend ratio, spin speeds or additives. The ratios can, however, vary greatly, which is why it is a good idea to do a test run of the polymer. The test is performed by having set spin speeds varying between 1k to 3k RPM. Then, a series of different D:A ratio, additives or annealing is performed. An example of first test is given below in Table 5.1

D:A		RPM		Annealed
1:1	1k	2k	3k	2k, 90°C /min
1:1.5	1k	2k	3k	
	1k 2%DIO	2k 2%DIO	3k 2%DIO	
1:2	1k	2k	3k	
	1k 3% CN	2k 3% CN	3k 3% CN	

Table 5.1: Overview of the parameter scan. First device is number 1, last device is number 16. CN:1-Chloronapthalene, DIO:1,8-Diiodooctane.

From this data it is possible to identify if any of the additives or treatments have an effect, while testing the optimal blend ration at the same time. Thus, from these parameters, the device data presented in Table 5.2 was obtained. The data is the best electrode from each device, statistics on the whole batch is presented beneath the table.

	V_{OC}	J_{SC}	FF	PCE
1	0.88	11.31	55.42	6.65
2	0.89	8.52	65.21	5.99
3	0.89	8.04	62.97	5.472
4	0.89	7.83	64.55	5.43
5	0.88	10.55	63.54	7.150
6	**0.89**	8.31	69.46	6.24
7	0.89	7.69	67.07	5.562
8	0.86	**11.78**	61.82	**7.56**
9	0.87	10.06	**70.61**	7.46
10	0.84	10.01	65.91	6.72
11	0.87	9.80	62.29	6.42
12	0.72	7.01	33.16	2.02
13	0.89	7.04	65.51	4.97
14	0.77	9.81	47.08	4.31
15	0.81	8.18	54.66	4.405
16	0.83	9.06	53.60	4.88

Table 5.2: Device photovoltaic results, the best in each column has been highlighted. The presented data is the best PCE obtained from each device.

As stated, the data presented in Table 5.2 is the best electrode from each device. The total statistic for the first batch is presented in Table 5.3.

	V_{OC}	J_{SC}	FF	PCE
Average	0.851	8.667	58.406	5.367
std dev	0.064	2.235	10.851	1.628
size	71	71	71	71
Margin of error	0.015	0.520	2.524	0.379
Bounds	0.851±0.015	8.667±0.520	58.406±2.524	5.367±0.379
Max	0.90	11.78	75.45	7.55
Min	0.56	0.30	22.47	0.04
Range	0.34	11.48	52.98	7.51

Table 5.3: Calculation of 95% confidence interval for the batch size of 71 working electrodes over 16 devices(damaged electrodes have been removed)

Already from the first parameter scan, 7.557% was achieved from device 8, which had been coated at 1k RPM and 2% DIO additive using a 1:1.5 D:A blend ratio. Which incidentially also achieved the highest J_{SC}, therefore, it was chosen as the "best cell", which would serve as a base for optimization. From the data it was evident that annealing and addition of CN did not have a positive effect on PV performance. Annealing on device 4 barely had an effect, but the PCE was lower than the matching device 2. CN did have a slightly lower PCE comparing device 14 to the nontreated device 11, where the PCE decreased 2%, and generally the FF was lower for the entire CN test. Due to the nature of OPVs, where the highest PCE obtained is the most interesting, coupled with the nature of statistics,

primarily confidence intervals, in which the highest and lowest ultima will be outside the 95% confidence interval. Therefore it is here only used to give a more general idea of the overall performance and reproducibility of the OPV devices, especially the FF which is an indicator of how well produced a device is.

As mentioned device 8 was chosen for further optimization, using the 1:1.5 D:A blend ratio, the next step was trying to optimize the DIO concentration and the spin speed for the experiment. Therefore, batch 2, device 17-32 was coated using 1:1.5 D:A, with varying spin speed from 0.75k to 1.5k RPM. Yielding 4 times 4 devices with same DIO concentration using 4 different spin speeds totalling 16 devices.

Device	V_{OC}	J_{SC}	FF	PCE
17	0.80	11.21	53.05	5.75
18	0.78	11.33	53.32	5.73
19	0.81	8.72	58.24	4.993
20	0.82	8.94	60.05	5.33
21	0.79	13.51	45.74	5.911
22	0.86	13.29	54.81	7.60
23	0.82	10.85	54.13	5.81
24	0.81	10.17	57.95	5.785
25	0.80	14.50	47.22	6.66
26	0.81	13.10	50.13	6.373
27	0.81	10.40	57.45	5.84
28	**0.875**	10.82	**67.06**	**7.65**
29	0.79	**17.81**	30.59	5.19
30	0.79	13.98	47.86	6.41
31	0.80	11.05	55.02	5.92
32	0.81	11.07	57.49	6.23

Table 5.4: Device data from Batch 2, changing DIO concentrations and RPM. The presented data is the best PCE obtained from each device. The highest of each parameter has been highlighted.

From the data represented in Table 5.4 it is evident that Device 28 is the best of this series. Device 28 was produced with 2.5% DIO and 1.5k RPM. To obtain a general overview of the entire batch, the overall statistics for the cells is presented in Table 5.5.

	V_{OC}	J_{SC}	FF	PCE
Average	0.810	11.580	51.909	5.762
std dev	0.034	2.000	8.371	0.878
size	81	81	81	81
Margin of error	0.007	0.436	1.823	0.191
Bounds	0.810±0.007	11.580±0.436	51.909±1.823	5.762±0.191
Max	0.94	17.81	67.06	7.65
Min	0.70	8.51	27.66	2.64
Range	0.24	9.30	39.40	5.01

Table 5.5: Calculation of 95% confidence interval for the batch size of 81 working electrodes over 16 devices(damaged electrodes have been removed)

As can be seen on the bounds, there is a smaller gap between the upper and lower bound,

but the average is lower than the first batch. The day this batch was made, there was an unusual high amount of oxygen in the glovebox, which, according to the lab personnel can have a large impact on the very thin active layer. The O_2 concentration was around 1200 ppm this day, as opposed to around 60 ppm the day the first batch was made. Despite the increased oxygen in the glovebox atmosphere, the best device proved to be 0.097% better than the best device from the first batch. Also a very high J_{SC} was observed from device 29 with a J_{SC} over 17 mA/cm^2, all of the electrodes from device 29 showed increased J_{SC}, as opposed to its much lower V_{OC}, FF and PCE. It was not possible to locate the cause for the increased J_{SC}. Which could normally be caused by the cords from each electrode touching each other during scan, however, this was not the problem here as the cords were freshly cut and the copper wiring was in place.

It was decided that another test was needed in order to try improving the results, while also trying to recreate the high PCE from device 28, and test if the mixture for device 29 would again yield a high J_{SC}. The test results obtained is presented in Table 5.6.

Device	V_{OC}	J_{SC}	FF	PCE
33	0.86	13.65	56.00	7.96
34	0.86	12.71	57.08	7.55
35	0.86	10.09	65.35	6.85
36	**0.87**	10.21	**67.31**	7.21
37	0.83	12.86	49.20	6.40
38	0.85	12.50	55.78	7.16
39	0.86	10.32	66.47	7.121
40	0.85	**14.04**	50.97	7.33
41	0.85	13.68	56.67	**8.02**
42	0.86	10.38	65.67	7.10
43	0.87	10.41	66.97	7.28
44	0.82	13.03	47.78	6.15
45	0.85	13.42	53.51	7.39
46	0.86	10.58	62.77	6.91
47	0.87	10.38	66.18	7.21

Table 5.6: Third batch of devices, containing device 33-47. Using the same parameters as in the second batch. The data presented data is the best PCE obtained from each device.

This batch was the last planned in QIBEBT, the amount of oxygen was low at the point of creation, and the electrodes was applied almost immediately after coating of the substrates. This batch included the hero cell of this project. It was estimated that the BDT-Pff donor moiety would be able to obtain about 8% PCE, which was also shown by Li *et al.* [2016] reaching a PCE of 8.24%, with a V_{OC} of 0.89V, a J_{SC} of 12.67 mA/cm^2 and a FF of 0.73.

Also, as can be observed in Table 5.6 11 out of 15 devices had a PCE performance of over 7%, their J_{SC} all above 10 mA/cm^2 and a steady V_{OC} on all devices.

The bounds for the second batch was given as 51.909±1.823, which means that there has been a slight increase in the FF, thus indicating that the amount of oxygen in the glovebox had an impact on the second batch, as both were treated equally, using DONOR, ACCEPTOR and solvent from the same bottles. Unfortunately there was not enough time to continue testing the devices, as device 41 could possibly be improved if the FF could

	V_{OC}	J_{SC}	FF	PCE
Average	0.846	11.691	57.974	6.832
std dev	0.025	1.398	7.218	0.651
size	70	70	70	70
Confidence coeff	1.96	1.96	1.96	1.96
Margin of error	0.006	0.327	1.691	0.152
Bounds	0.846±0.006	11.691±0.327	57.974±1.691	6.832±0.152
Max	0.87	14.03	67.31	8.01
Min	0.73	9.89	43.13	4.94
Range	0.14	4.14	24.18	3.07

Table 5.7: Statistical data for the third batch using 95% confidence.

be increased. From this knowledge it was concluded that device 33 and 41 were the best performing devices, and they were chosen for EQE and thickness measurement.

BDT has been proved to be a well performing donor backbone moiety for OPV. Chen *et al.* [2015], reported that a 7.02% PCE was achieved by introducing a single fluorine atom on both benzene branching from the BDT backbone, processing the cells with a D:A of 1:1 w/w and a 0.5% DIO additive. Another group, Yuan *et al.* [2013], reported that a similar structure PBDTPO-DTBT, without any fluorine atoms achieved a maximum PCE of 3.4%. Using a D:A blend of 1:2, this was, however, with a FF below 50% and without additive, the sidechains on the DTBT unit was also located on the benzene ring, whereas the acceptor unit DTBT used in Chen *et al.* [2015] and this project utilized branched sidechains located on the thiophene part of DTBT. Gao *et al.* [2014] reported that their polymer 14, using an identical DTBT acceptor with sidechains located on the thiophene units, managed to achieve an astounding 8.07% PCE, the group reported a FF of 70.9% which could explain the high effiency. Gao *et al.* [2014]s group was using a D:A blend 1:1.5 and 0.5% DIO additive, which was almost the same method utilized for the highest PCE device in this report. Gao *et al.* [2014] also mentions that they believe the PBDT-DTBT derivatives would break the 10% PCE milestone within short time. For the device 41 prepared in this project, it is believed that if the FF could be improved, increased from 56%, to 70+% there would be a substantial increase in performance.

5.1.2 I-V data

The calculation of PCE is performed from the voltage and current measurements done in the device lab. Usually the software also includes calculations of the FF and PCE, but it can also be calculated by hand using I-V plots, plotting a reversed current vs voltage to yield a graph like Figure 5.1.

The largest PCE is found at the optimized I and V, for the largest possible value, as explained from the Equation 1.1, to calculate the PCE, the FF is also needed, which is found from the intersection of both axes, and comparing it with the maximum area from the voltage and current inside the graph. As shown in Figure 5.2 the squares has been drawn, using orange for device 9 and blue for device 41.

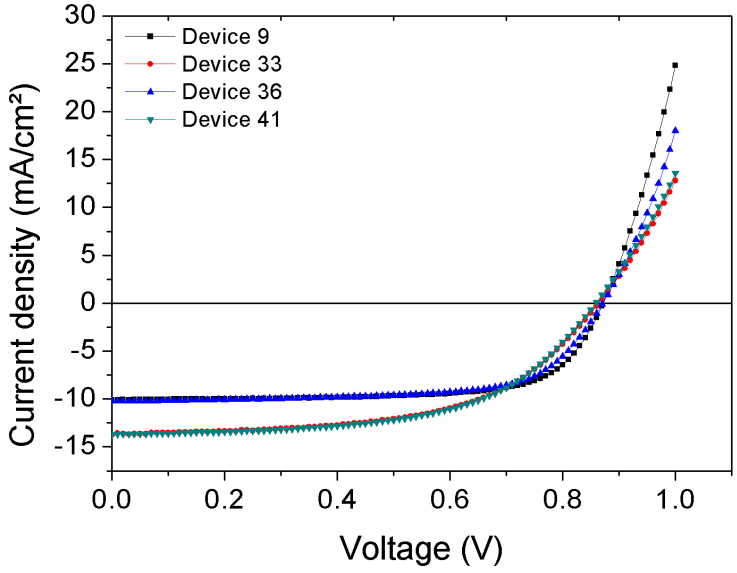

Figure 5.1: IV plot showing performance for device 9, 33, 36 and 41. Device 9 and 36 exhibit lower PCE but a higher FF, compared to device 33 and 41 which has a high PCE performance, but FF only around 55%.

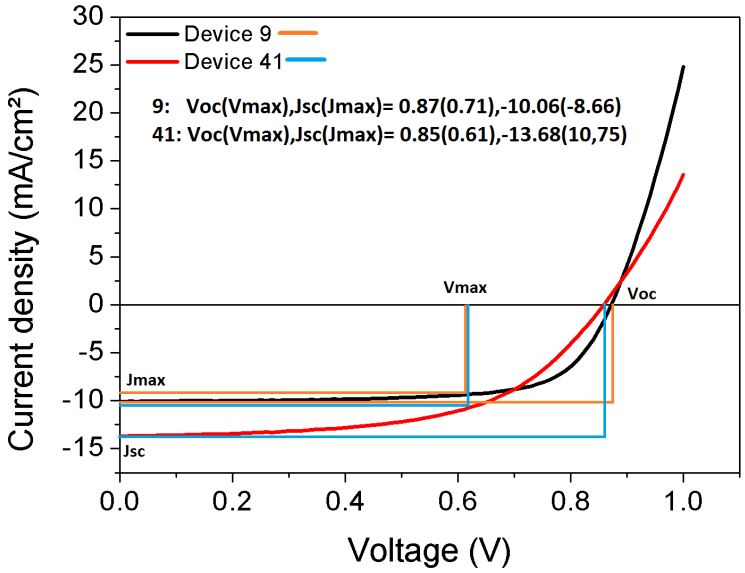

Figure 5.2: IV plot of device 9 and 41, with V_{max}, V_{OC}, J_{max} and J_{SC} depicted.

The calculation of FF is given by the Equation 5.1.

$$FF = \frac{J_{max} \times V_{max}}{J_{SC} \times V_{OC}} \tag{5.1}$$

$$FF_9 = \frac{8.66 mA/cm^2 \times 0.71V}{10.06 mA/cm^2 \times 0.87V} \times 100\% = 70.25\%$$

$$FF_{41} = \frac{10.75A/cm^2 \times 0.61V}{13.68mA/cm^2 \times 0.85V} \times 100\% = 56.39\%$$

The method for finding J_{max} and V_{max} is to calculate the power out from the cell at each voltage, using P=VI thus giving power on the y axis plotted against voltage in the IV plot, an example of this graph can be observed in Figure 5.3

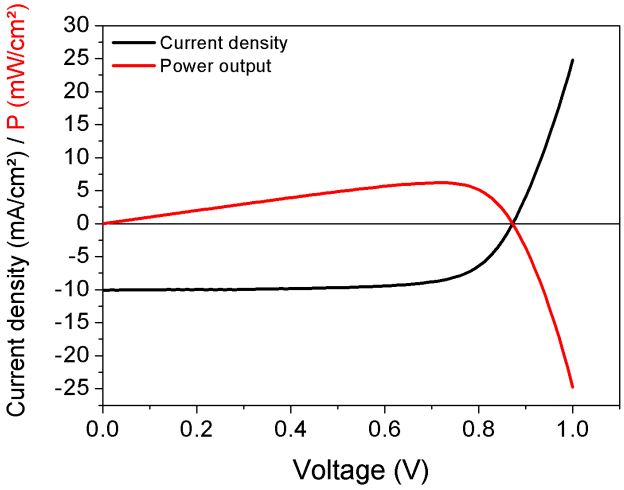

Figure 5.3: Current density and power output for device 9, plotted against voltage.

Given this information it is possible to calculate the V_{max} and J_{max}, as the highest point on the power output graph, which is the highest power obtainable, which marks the V_{max} spot on the axis, if a line is drawn directly down to the current density graph, the intersection with the graph marks the J_{max} on the y axis. Which can then be used to calculate FF and PCE at the highest output.

5.1.3 UV-VIS

The UV-vis was prepared by $CHCl_3$ solution and the film by casting a concentrated polymer solution in $CHCl_3$.

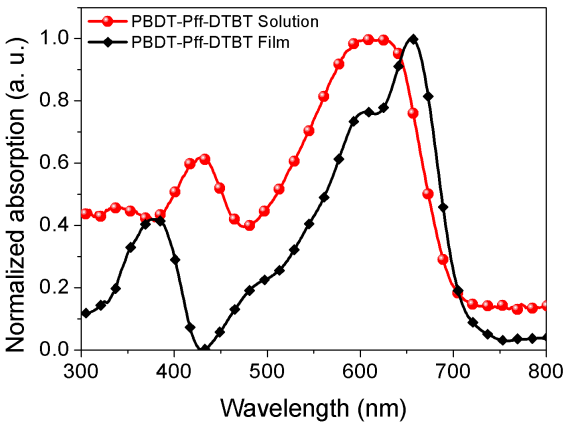

Figure 5.4: UV-vis of PBDT-Pff-DTBT in $CHCl_3$ solution and as a coated film.

Overall the polymer exhibits two absorption bands between 300-700nm. The excitation energy decreases at higher wavelengths, the high energy absorption like $\pi - \pi*$ transitions are in the lower wavenlength region, while the lower energy transitions, like intramolecular charge transfer happening from donor to acceptor is visible in the higher wavelength region [Reusch, n.d.] [Piliego & Loi, 2012]. The solution of PBDT-Pff-DTBT exhibit a good absorption in the UV spectrum and the short wavelength region of the visible spectrum a peak is visible with onset around 380nm, peak at 430nm and ending at 460nm, which is around the onset of the primary peak in the high wavelength end of the visible spectrum. The casted film exhibited a lower absorption in the UV and near UV range, with near transparancy at 430nm, both Chen *et al.* [2015] and Yuan *et al.* [2013] reported a strong decrease in the film absorption, the fluorinated moiety from Chen *et al.* [2015] had the decrease at 475nm, dipping the absorbance to around 0.35. The nonfluorinated moiety reported by Yuan *et al.* [2013] had the decrease around 370nm. None of the mentioned polymers gave any indication of whether the Pff species had blue shifted its solution peak at 430nm to give the film peak at 380nm, or if this is a different peak. The primary peak in the film is slightly red shifted compared to the primary peak of the solution. The primary film peak possesses a blue shifted shoulder, which was also reported by Yuan *et al.* [2013] but was not commented further on. The higher visible end shows a red shift in the film compared to the film, however, the onset of the peaks are around the same point, which could give an indication that the $\pi - \pi$ stacking is present already in the solution due to aggregation seen in bulky polymer systems [Amrutha & Jayakannan, 2008].

The film of PBDT-Pff-DTBT has an absorption edge onset at 720nm, which is equal to a bandgap of 1.725eV, which is a little lower than the single fluorinated moiety reported by Chen *et al.* [2015] at 1.73eV, and higher than the bandgap reported by the nonfluorinated moiety by Yuan *et al.* [2013] which was reported at 1.62eV. Li *et al.* [2016] found a bandgap of 1.81 eV for the polymer most like the PBDT-Pff polymer of this project.

5.1.4 External Quantum Efficiency

EQE was measured for device 33 and 41 in order to determine what current the device produces when absorbing light at various wavelengths.

The EQE can be used to calculate J_{SC} as described in Equation 2.1 by integrating over the entire range of wavelengths absorbed. This number is the theoretical estimation of J_{SC}. Using Equation 2.1 to calculate yields a J_{SC} of 13.0 mA/cm^2 for device 33 and 10.6 mA/cm^2 for device 41. Both of these values however are lower than the originally measured J_{SC} data during device testing, 13.66 mA/cm^2 and 13.68 mA/cm^2 respectively. While the estimation for device 33 is close to the device measurement, the estimate for device 41 is not. This discrepancy could, however, be explained in the way the EQE is measured as even a small difference in the positioning of the sample can drastically effect the EQE measurement. The EQE study also shows the compensation of the ACCEPTOR material on the light absorption around 440nm compared to the almost transparent absorption at 440nm of the DONOR material. The single fluorinated polymer from Chen *et al.* [2015]s results showed similar decreases around 500nm, their polymer showed an onset around 725nm and maximum EQE around 70% which is very similar to the polymer researched in this report. The non fluorinated moiety reported by Gao *et al.* [2014] also gave a

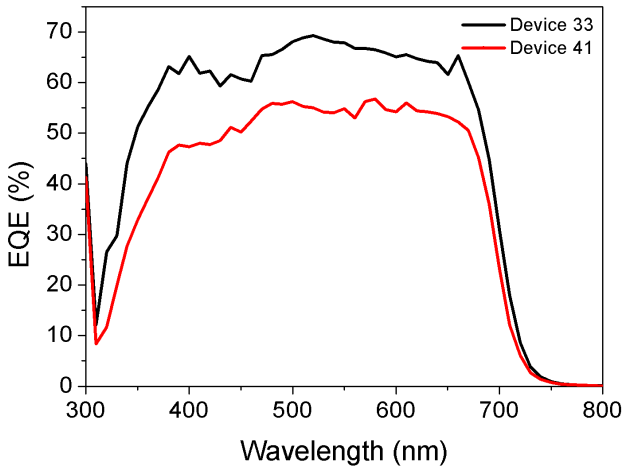

Figure 5.5: EQE data for device 33 and 41.

decrease in the EQE at 400-420nm, although their onset and maximum EQE is not as high, capping at 60% and onset around 690nm.

5.1.5 Cyclic Voltammetry

The CV measurements were made at Aarhus University, department of Engineering. The method used was a three electrode setup with a glassy carbon working electrode, which was coated with polymer, a platinum counter electrode and an Ag/Ag^+ pseudo reference electrode, the electrolyte setup was 0.1M Bu_4NBF_4 in Acetonitrile.

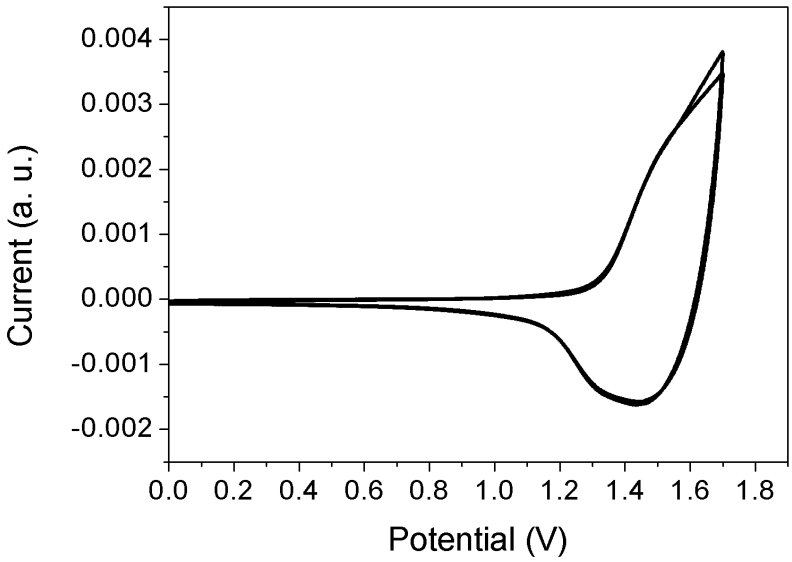

Figure 5.6: Cyclic voltammogram of casted film vs SCE in 0.1M Bu_4NBF_4 in Acetonitrile solution.

The CV oxidation onset is used to calculate the HOMO level of the donor moiety. The HOMO and LUMO level can be calculated from the equation reported by [Leonat *et al.*,

2013].

$$E_{HOMO} = -(E_{Ox}^{onset} + 4.4) \tag{5.2}$$

$$E_{LUMO} = -(E_{Red}^{onset} + 4.4) \tag{5.3}$$

A scan was performed, but no reduction peak was present, therefore, another approach for obtaining the LUMO level was needed. By calculating the HOMO level from the oxidation onset, and adding the bandgap obtained from UV-vis, the LUMO energy of the material can be obtained. Using Equation 5.2 and the onset vs SCE can be obtained from the CV plot, in this case the onset is around 1.3V, and by inserting this into the equation we obtain the HOMO level and adding the bandgap from UV-Vis, the LUMO level for the polymer is obtained.

$$E_{HOMO} = -e(1.3V + 4.4) = -5.7eV$$

$$E_{LUMO} = -5.7 + 1.725 = -3.975eV$$

Comparing these data to the beforementioned papers from Chen *et al.* [2015] who reported HOMO(LUMO);bandgap to be -5.39eV(-3.66eV);1.73eV. Yuan *et al.* [2013] reported -5.46eV(-3.66eV);1.8eV and the nonfluorinated moiety made by Gao *et al.* [2014] exceeding 8% PCE was reported to have a HOMO level of -5.35eV. Which is an indication towards the PBDT-Pff-DTBT exhibiting a very deep HOMO level, which can explain the high V_{OC} even with low FF, giving an indication of greater potential than what the polymer has already shown.

5.1.6 Morphology

A selection of devices from the first batch and 2 devices from the last batch, were chosen for Atomic force microscope (AFM) to observe how changes in the blend would change the morphology, in order to better understand the FF and thereby the PCE of the devices. The AFM pictures were made on an Ntegra(NT-MDT) AFM, using silicon tip cantilevers (NSG10, NT-MDT) in tapping mode with a frequency of 0.5 Hz to create a 256x256 pixel image of 3x3µm. Gwyddion was used to afterprocess the images, by leveling them with plane subtraction to obtain a leveled image, the same software was used to calculate the surface roughness of the entire sample.

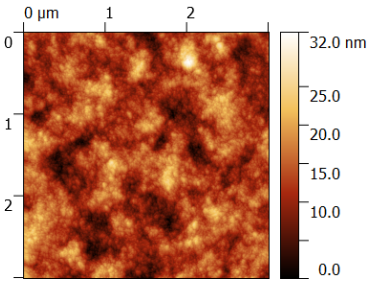

Figure 5.7: Device 1, with a RMS surface roughness of 4.19nm.

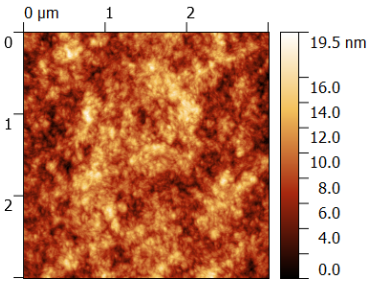

Figure 5.8: Device 4, with a RMS surface roughness of 4.77nm.

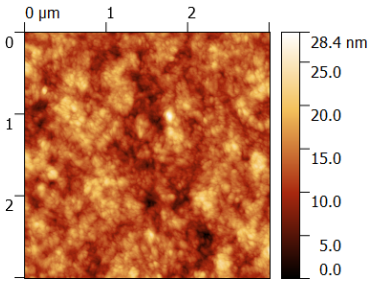

Figure 5.9: Device 5, with a RMS surface roughness of 3.31nm.

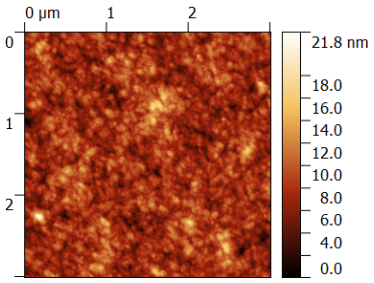

Figure 5.10: Device 7, with a RMS surface rougness of 2.11nm.

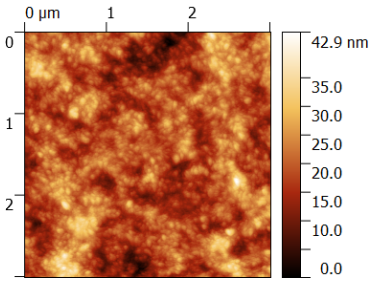

Figure 5.11: Device 8, with a RMS surface roughness of 5.44nm.

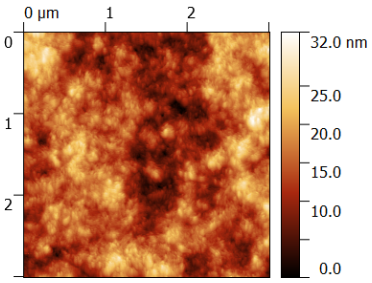

Figure 5.12: Device 14, with a RMS surface roughness of 4.77nm.

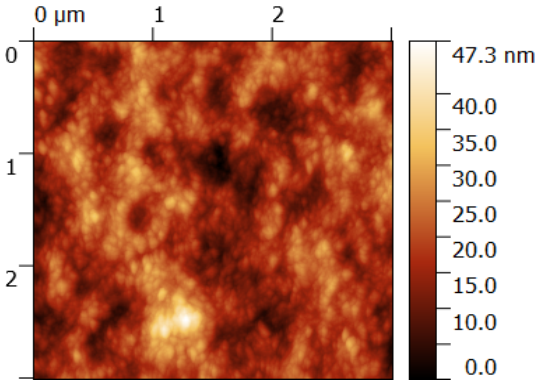

Figure 5.13: Device 33, with a RMS surface roughness of 5.83nm.

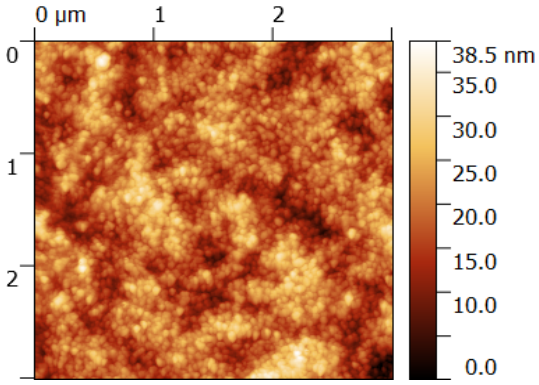

Figure 5.14: Device 41, with a RMS surface roughness of 5.08nm.

To sum up the parameters and the results, the data is put into a table.

Device	Blend	RPM	additive/anneal	RMS roughness	FF [%]	PCE [%]
1	1:1	1k		4.19	55.422	6.657
4	1:1	2k	90°/10min	4.77	64.551	5.439
5	1:1.5	1k		3.31	53.541	7.150
7	1:1.5	3k		2.11	67.070	5.562
8	1:1.5	1k	2% DIO	5.44	61.823	7.557
14	1:2	1k	3% CN	4.77	47.082	4.317
33	1:1.5	0.75k	1.5% DIO	5.83	56.003	7.960
41	1:1.5	1k	2.5% DIO	5.08	56.677	8.018

Table 5.8: Crafting parameters of the devices that AFM was performed on, compared to their RMS surface roughness in nm

From the data presented in Table 5.8 it seems that the primary parameter for film roughness is the spinspeed during coating, thus, device 7 coated at 3k RPM possesses a much lower RMS roughness at 2.11nm, the FF is also the highest on device 7 compared to the other AFM samples, although the PCE is only at 5.562%. Annealing does not indicate to have a positive impact on any of the factors. CN did have a lower roughness, than its counterpart with DIO, however a difference in PCE at over 3%, it would not be worth testing further on. Comparing device 5 and 41, it seems that the addition of DIO

increased the roughness from 3.31nm to 5.08, while also increasing the PCE by almost 1%, while keeping FF at almost the same value. This is interesting since Chen *et al.* [2015] reported that after the addition of 0.5% DIO, the RMS roughness decreased from 4.8nm to 3.5nm, while improving the FF almost 20% and PCE with over 2.5%. Min *et al.* [2012] found that the morphology was improved alot with the addition of 5% DIO, with the visible "particles" in the AFM decreasing in diameter going from 1µm to about 100nm. and the difference in the surface decreased by 50% going from max 34.71nm to max 15.27nm in the DIO sample. Therefore the AFM could indicate that further studies in the morphology of the polymer PBDT-Pff-DTBT might be in order, but also try obtaining a high PCE with supporting high FF and receive the AFM data from that device, to see how it would affect the general picture and the RMS roughness.

5.2 PBDT-TS and PBDT-FS polymers

The four polymers PBDT-TS-TPD, PBDT-FS-TPD, PBDT-TS-PTPD and PBDT-FS-PTPD were all synthesised, but neither of the PTPD polymers showed any useful results devices were only made from PBDT-TS-TPD and PBDT-FS-TPD. UV-VIS spectra as well as SEC was done for both, and UV-VIS was attempted for all four, but PBDT-TS-PTPD could not be dissolved sufficiently to gain a spectra.

5.2.1 Size exclusion chromatography

Size exclusion chromatography envelops smaller particles, and thus, larger particles have lower retention time. A standard curve was made using Polystyrene standards from American polymer standard service in different degrees of polymerization permeating though a gel column. For this experiment polystyrene standards with an average molecular weight of 2900, 9580, 42900, 188000 and 451000 g/mol was used. The retention times obtained from the experiment is plotted in Figure 5.15

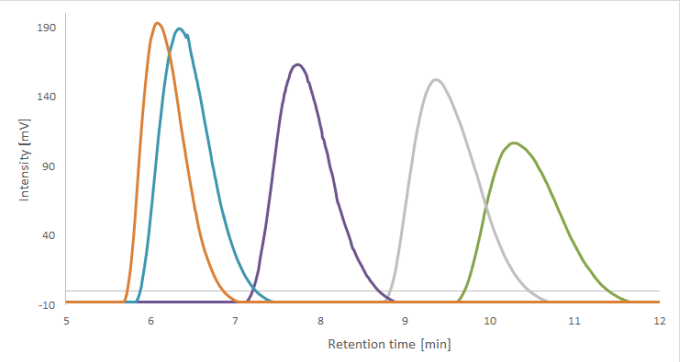

Figure 5.15: Retentionplot of polysterene polymers, in decreasing size for longer retention.

In order to produce the standard curve, the retention time is noted for each maximum, and these data are plotted against their respective molecular weight, the standard curve is obtained. To the left the standard plot is given, and to the right the first order representation of the data with regression plot.

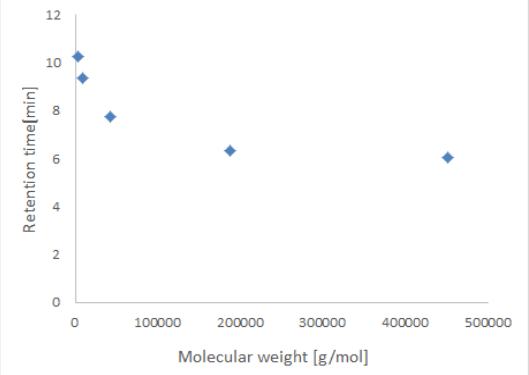

Figure 5.16: Standard curve from Polystyrene polymers.

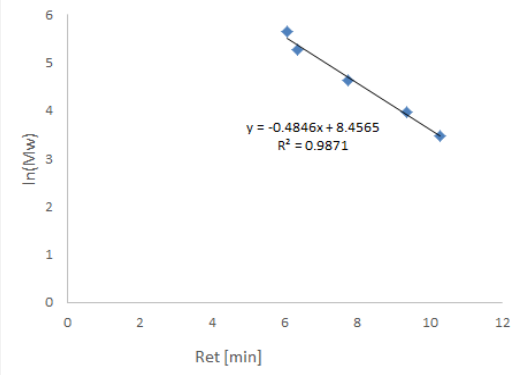

Figure 5.17: First order representation of the standard curve with regression plot.

From the First order equation given, we can calculate an approximate molecular weight for PBDT-TS/FS-TPD. The retention time of the local maxima from the HPLC output is noted, and used in the equation obtained in Figure 5.17.

$$ln(Mw) = -04846x + 8.4565 \tag{5.4}$$

Using equation Equation 5.4 and isolating Mw, the molecular weight of the polymer fractions can be obtained. PBDT-TS-TPD has 2 peaks, one at 9.0008 min and a much smaller one at 10.897 min. All the HPLC data is in Table 5.9.

Polymer	retention time [min]	Estimated Mw	D_p
PBDT-FS-TPD	9.0140	12255	14
PBDT-TS-TPD	9.0008	12437	13.7
PBDT-TS-TPD	10.8970	1499.04	1.6

Table 5.9: Size exclusion data for synthesized polymers.

The degree of polymerization (D_p) is not very large, however, the synthesized polymers are already larger than Polystyrene that has a Mw of 104.1 g/mol per repeating unit, with the synthesized BDT based polymers exceeding 870 g/mol per repeating unit, going as high as 1530 g/mol per repeating unit for BDT-Pff-DTBT.

5.2.2 Absorption data

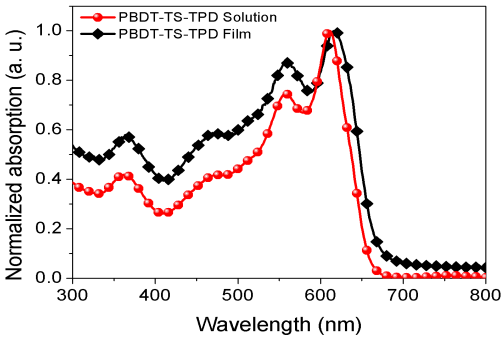

Figure 5.18: UV-VIS data of PBDT-TS-TPD

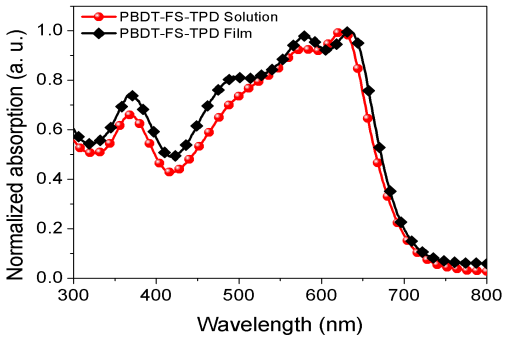

Figure 5.19: UV-VIS data for PBDT-FS-TPD

The PBDT-TS-TPD polymer film has a cutoff point for the absorbtion spectra around 670 nm which can be use to calculate bandgap energy (E) as shown in Equation 5.5.

$$\frac{6.626 \times 10^{-34} \times 3 \times 10^{8}}{670 \times 10^{-9}} = 2.966 \times 10^{-19} \tag{5.5}$$

Since bandgap energy is usually given in eV the conversion: $1.6 \times 10^{-19} = E$ is used giving:

$$\frac{2.966 \times 10^{-19}}{1.6 \times 10^{-19}} = 1.854eV \tag{5.6}$$

Using the same calculations for PBDT-FS-TPD which has a cutoff point around 700 nm.

$$\frac{6.626 \times 10^{-34} \times 3 \times 10^{8}}{710 \times 10^{-9}} = 2.799 \times 10^{-19}$$

$$\frac{2.799 \times 10^{-19}}{1.6 \times 10^{-19}} = 1.75eV$$

J_{SC} is assumed to be primarily influenced by the bandgap, with a more narrow bandgap yielding a higher J_{SC} as described in Section 1. Thus based on the UV-VIS data PBDT-FS-TPD should have the highest J_{SC} of the two.

Although no device data was obtained for PBDT-FS-PTPD the theoretical bandgap was still calculated from absorption.

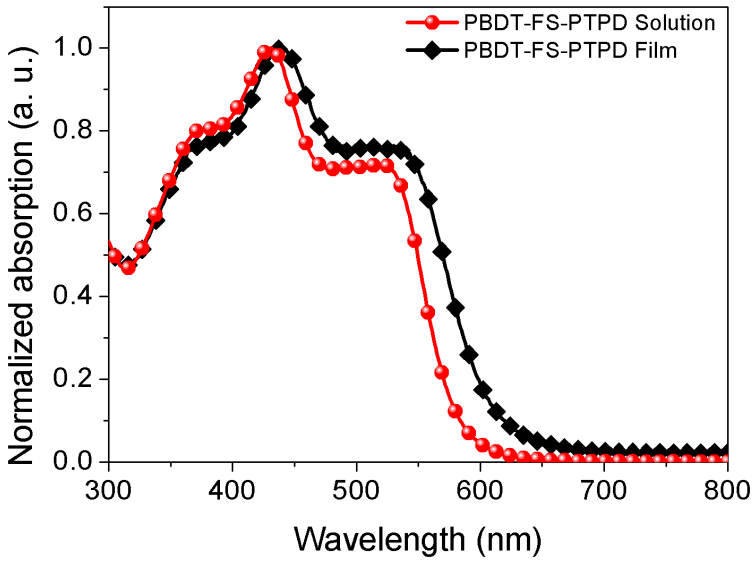

Figure 5.20: UV-VIS data for PBDT-FS-PTPD as both film and solution.

$$\frac{6.626 \times 10^{-34} \times 3 \times 10^{8}}{620 \times 10^{-9}} = 3.206 \times 10^{-19}$$

$$\frac{3.206 \times 10^{-19}}{1.6 \times 10^{-19}} = 2.00eV$$

This is a much larger bandgap than the other polymers studied in this project and can easily explain why no device data could be obtained, as it simply might not absorb enough energy to excite its electrons.

5.2.3 Device data

Both PBTD-FS-TPD and PBTD-TS-TPD were used for BHJ devices in which they acted as the DONOR while $PC_{60}BM$ was used as the ACCEPTOR. Initially PBTD-FS-TPD was tested at different blend ratio between DONOR and ACCEPTOR, with 1:1.5 showing the best results as shown in Figure 5.21.

AAUPO1 Acceptor: $PC_{60}BM$ 30mg/mL Solvent: DCB

	Voc	Jsc	FF	PCE
1:1	0.929	3.72	45.78	1.58
1:1.5	0.929	3.64	47.22	1.60
1:2	0.931	2.90	56.19	1.52

AAUPO1 D/A Blend ratio: 1:1.5 Acceptor: $PC_{60}BM$ 30mg/mL Solvent: DCB

	Voc	Jsc	FF	PCE
Anneal at 70℃	0.936	3.48	47.18	1.54
0.5%DIO	0.893	5.55	40.28	2.00
1%DIO	0.888	5.56	42.13	2.08
2%DIO	0.881	5.35	38.80	1.83

AAUPO1 D/A Blend ratio: 1:1.5 Acceptor: $PC_{70}BM$ 30mg/mL Solvent: DCB

	Voc	Jsc	FF	PCE
Without DIO	0.923	3.59	46.91	1.55
1%DIO	0.841	6.26	40.94	2.15

Figure 5.21: Device data for PBTD-FS-TPD best results being with 1:1.5 D:A blend ratio, 1% DIO and using $PC_{70}BM$

The devices were also tested for the effect of annealing as well as with the addition of DIO, with the highest obtained PCE being 2.08% on a device with 1% DIO. Finally the ACCEPTOR was changed from $PC_{60}BM$ to $PC_{70}BM$, which led to the highest performance of 2.15%.

AAUPO2 Acceptor: $PC_{60}BM$ Concentration: 30mg/mL Solvent: DCB

Polymer/PC60BM	Voc	Jsc	FF	PCE
1:1	1.06	4.61	44.67	2.19
1:1.5	1.04	5.46	50.57	2.87
1:2	1.03	4.85	50.63	2.52

AAUPO2 D/A Blend ratio: 1:1.5 Acceptor: $PC_{70}BM$ 30mg/mL Solvent: DCB

	Voc	Jsc	FF	PCE
Without DIO	1.02	6.66	52.90	3.57
1%DIO	1.01	7.32	55.05	4.05

Figure 5.22: Device data for PBTD-TS-TPD best results being with 1:1.5 D:A blend ratio and 1% DIO

The same conditions proved to be optimal for PBTD-TS-TPD with a 1:1.5 ratio blend, $PC_{70}BM$ and 1% DIO. However, the PCE of all tested devices were higher than those of PBTD-FS-TPD, with the best result being 4.05% PCE.

Specifically comparing Figure 5.21 and Figure 5.22, PBTD-TS-TPD has higher V_{OC}, which could be connected to a deeper HOMO level of the donor, a higher J_{SC} meaning better exciton forming properties and a higher fill factor which is often connected to a better morphology of the device surface. The most surprising of these results is the J_{SC} because as shown in Section 5.2.2, the PBTD-FS-TPD polymer had a lower bandgap which should facilitate easier exciton formation leading to higher J_{SC}. Since the J_{SC} did not match the

expectations based on absorption spectra there might be some other factors aside from the bandgap that influences the J_{SC} that might be detectable by analysing the EQE, which was unfortunately not done for this project. The higher V_{OC} for the PBTD-TS-TPD was expected due to the electron density difference giving a deeper HOMO level as described in Section 2.3.

6 | Conclusion

The synthesis of PBDT-Pff-DTBT and PBDT-Pff-DPP was succesfully completed, but since PBDT-Pff-DPP could not be dissolved, only PBDT-Pff-DTBT was applied for device fabrication. The devices generally performed well with an average PCE of 5.367% for the first batch, 5.82% for the second batch and 6.832% for the final batch. The best device showed a PCE of 8.02% with a V_{OC} of 0.85V, a J_{SC} of $13.68 mA/cm^2$ and a FF of 56.57%. This is a very high PCE for an OPV device and could be improved by obtaining a better Fill factor.

UV-VIS spectra for PBDT-Pff-DTBT were made for both the solution and film presenting a bandgap of 1.725eV. Cyclic voltammetry was applied to determine the HOMO level of the polymer which showed a deep HOMO of -5.7eV. Finally, AFM pictures found that morphology had a large impact on the fill factor of the devices.

Regarding the difference between furan and thiophene when used in a BDT-based polymer for OPVs, it it quite clear that the devices made from the thiophene substituted polymer had a better performance, with a PCE almost twice as high as that of the furan substituted one. The TS-polymer had a higher V_{OC}, J_{SC} and Fill factor. The absorption spectra of each polymer showed that the FS should have a more narrow bandgap, but the J_{SC} was still less than for TS, which might explained by studying the EQE for both. The higher V_{OC} was expected however, since oxygen is better at delocalising its lone pair.

Overall it is clear, from both experiments with BDT-FS, BDT-TS and BDT-Pff, that the electron density of the aromatic system in the donor is of great importance to the performance of the OPV.

7 | Perspective

The results of this project opens up for several new inquiries into the behaviour of photovoltaic devices. First of all the devices made using BDT-Pff-TPD as DONOR could reach 8% even with just a few optimisations, it might be possible to reach even higher PCEs by simply optimizing the device fabrication further, especially by increasing FF. Additionally, if substituting two fluorine atoms onto the phenol sidechains of the BDT can yield a PCE of 8% what might be the effect of further altering the electron density in the phenol sidechains. There is also the question whether another acceptor for the D-A copolymer could yield better charge separation and transport which might also improve the performance of the device. It might even be possible to optimize the ACCEPTOR in case a better one can be found to replace $PC_{70}BM$. Finally there is a question of scaling, whether the devices can be made using more large scale fabrication methods such as roll to roll. And if it can, what the expected lifetime of a device.

Regarding the BDT-FS and BDT-TS experiments, further study is also required in order to determine the cause of the large PCE difference between the two. Measuring the EQE of the devices could explain why BDT-TS outperformed BDT-FS on J_{SC} despite the latter having a more narrow bandgap. Cyclic voltammetry could give an estimate of the HOMO/LUMO levels of each polymer which would also help explain the differences. Overall, more testing and analysis of the effects of structure on performance would be a good way to allow a more rational design approach towards making new polymers for OPV.

Bibliography

Amrutha, S. R., & Jayakannan, M. 2008. Probing the pi-Stacking Induced Molecular Aggregation in pi-Conjugated Polymers, Oligomers, and Their Blends of p-Phenylenevinylenes. *Journal of Physical Chemistry B*, **112**, 1119–1129. 36

Bao, Zhenan, Chan, Wai Kin, & Yu, Luping. 1995. Exploration of the Stille Coupling Reaction for the Syntheses of Functional Polymers. *Journal of American Chemical Society*, **117**, 12426–12435. 18

BP. 2014. *BP Statistical Review of World Energy June 2014*. Tech. rept. 9

Chen, Weichao, Du, Zhengkun, Han, Liangliang, Xiao, Manjun, Shen, Wenfei, Wang, Ting, Zhou, Yuanhang, & Yang, Renqiang. 2015. Efficient polymer solar cells based on a new benzo[1,2-b:4,5b']dithiophene derivative with fluorinated alkoxyphenyl side chain. *Journal of Materials Chemistry A*, 3130. 21, 33, 36, 38, 40

Gao, Chen, Wang, Liwei, Li, Xiaoyu, & Wang, Haiqiao. 2014. Rational design on D-A conjugated P(BDT-DTBT)polymers for polymer solar cells. *Polymer Chemistry*, 5200–5210. 33, 36, 38

He, Feng, Wang, Wei, Chen, Wei, Xu, Tao, Darling, Seth B., Strzalka, Joseph, Liu, Yun, & Yu, Luping. 2011. Tetrathienoanthracene-Based Copolymers for Efficient Solar Cells. *Journal of the American Chemical Society*, 3284–3287. Methods and Materials found in Supporting Information for paper. 23

Kirchmeyer, Stephan, & Reuter, Knud. 2005. Scientific importance, Properties and growing applications of poly(3,4-ethylenedioxythiophene. *Journal of Materials Chemistry*. 11

Larsen-Olsen, Thue T., Dam, Henrik F., Andreasen, Birgitta, Tromholt, Thomas, & Krebs, Frederik C. 2011. Polymersolceller. *Kemiåret 2011*. 9

Leonat, Lucia, Sbarcea, Gabriela, & Branzoi, Ioan Viorel. 2013. CYCLIC VOLTAMMETRY FOR ENERGY LEVELS ESTIMATION OF ORGANIC MATERIALS. *Scientific Bulletin B*, **3**, 111–118. 37

Li, Guangwu, Gong, Xue, Zhang, Jicheng, Liu, Yahui, Feng, Shiyu, Li, Cuihong, & Bo, Zhishan. 2016. 4-Alkyl-3,5-difluorophenyl-Substituted Benzodithiophene-Based Wide Band Gap Polymers for High-Efficiency Polymer Solar Cells. *Applied Materials & Interfaces*. 32, 36

McMurry, John. 2011. *Fundamentals of Organic Chemistry*. 16

Miles, Robert W., Zoppi, Guillaume, & Forbes, Ian. 2007. Inorganic photovoltaic cells. *Materials Today*, **10**(11), 20–27. 9

Min, Jie, Zhang, Zhi-Guo, Zhang, Siyuan, & Li, Yongfang. 2012. Conjugated Side-Chain-Isolated D-A Copolymers Based on Benzo[1,2-b:4,5-b']dithiophene-alt-dithienylbenzotriazole: Synthesis and Photovoltaic Properties. *Chemistry of Materials*, 3247–3254. 40

Piliego, Claudia, & Loi, Maria Antonietta. 2012. Charge transfer state in highly efficient polymer-fullerene bulk heterojunction solar cells. *Journal of Materials Chemistry*, 4141–4150. 36

Reusch, William. *Visible and Ultraviolet Spectroscopy.* 36

Savenije, Tom J. *Organic Solar Cells, Chapter 8. Excitron Solar cells.* 12

Schlatmann, A. R., Floet, D. Wilms, Hilberer, A., Garten, F., Smulders, P.J.M., Klapwijk, T.M., & Hadziioannou, G. 1996. Indium contamination from the indium-tin-oxide electrode in polymer light-emitting diodes. *Applied Physics Letters.* 11

Scott, J.C., Kaufman, J.H., Brock, P.J., DiPietro, R., Salem, J., & Goitia, J.A. 1996. Degradation and failure of MEH-PPV light-emitting diodes. *Journal of Applied Physics.* 11

Secaites, Jonathan D., Ratner, Mark A., & Marks, Tobin J. 2009. Practical efficiency limits in organic photovoltaic cells: Functional dependence of fill factor and external quantum efficiency. *Applied Physics Letters.* 12

Spanggaard, Holger, & Krebs, Frederik C. 2004. A brief history of the development of organic and popolymer photovoltaics. *Solar Energy Materials & Solar Cells.* 11, 12, 13

Spivey, Alan C. 20112. *Heteroaromatic Chemistry Lecures 4 & 5 - Pyrroles, furans & thiophenes - properties syntheses & reactivity.* 19

Ward, Chris Llewellyn Smith & David. 2008. Fusion. *Energy Policy.* 9

Yuan, Jun, Xiao, Lu, Liu, Bo, Li, Yongfang, He, Yuehui, Pan, Chunyue, & Zou, Yingping. 2013. New alkoxylphenyl substituted benzo[1,2-b:4,5-b0]dithiophene-based polymers: synthesis and application in solar cells. *Journal of Materials Chemistry A*, 10639–10645. 33, 36, 38

Zhou, Huaxing, Yang, Liqiang, Stuart, Andrew C., Price, Samuel C., Liu, Shubin, & You, Wei. 2011. Development of Fluorinated Benzothiadiazole as a Structural Unit for a Polymer Solar Cell of 7 *Angewandte Chemie, International Edition*, **50**, 2995–2998. 10, 19

Zhou, Huaxing, Yang, Liqiang, & You, Wei. 2012. Rationel Design of High Performance Conjugated Polymers for Organic Solar Cells. *Macromolecules.* 9, 10, 12, 21

A | NMR data

A.1 NMR data for compound 1

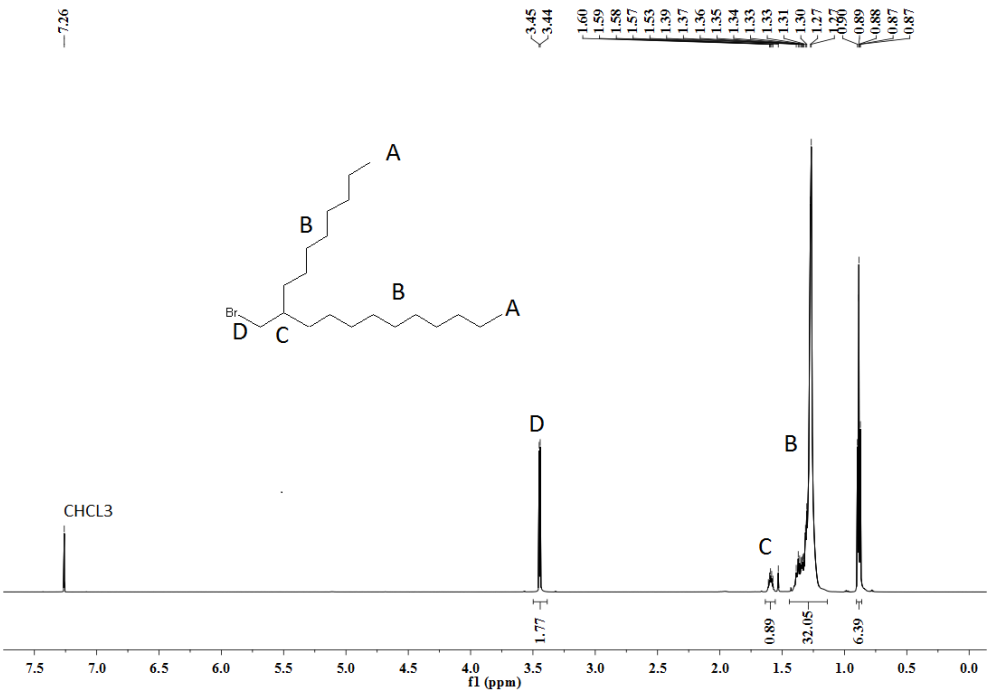

Figure A.1: H-NMR, 600 MHz.

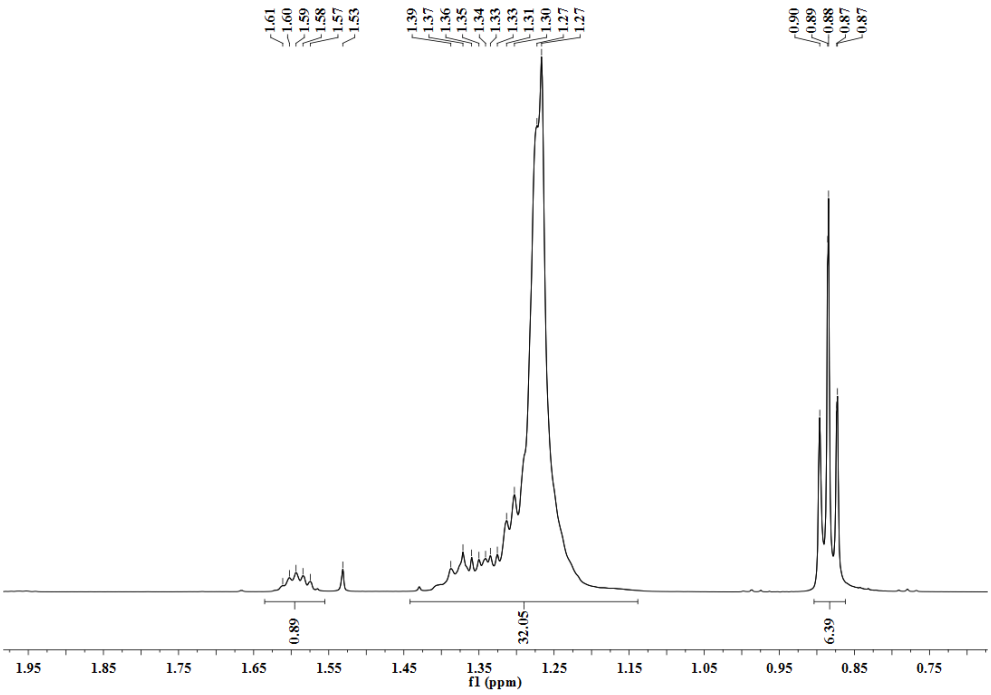

Figure A.2: H-NMR, 600 MHz.

A.2 NMR data for compound 2

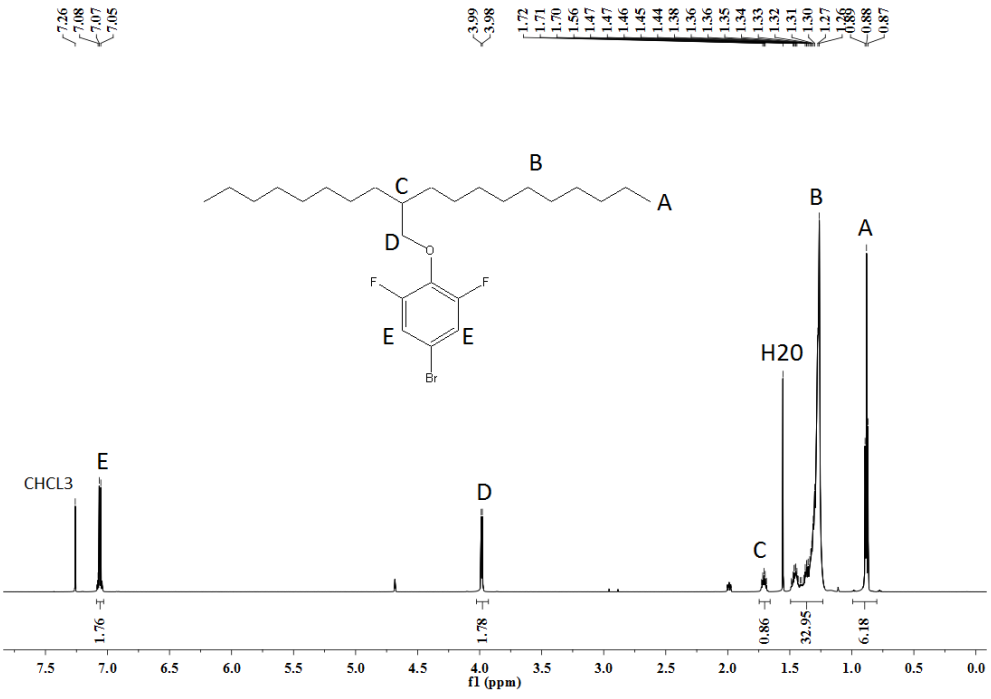

Figure A.3: H-NMR, 600 MHz.

A.3 NMR data for compound 3

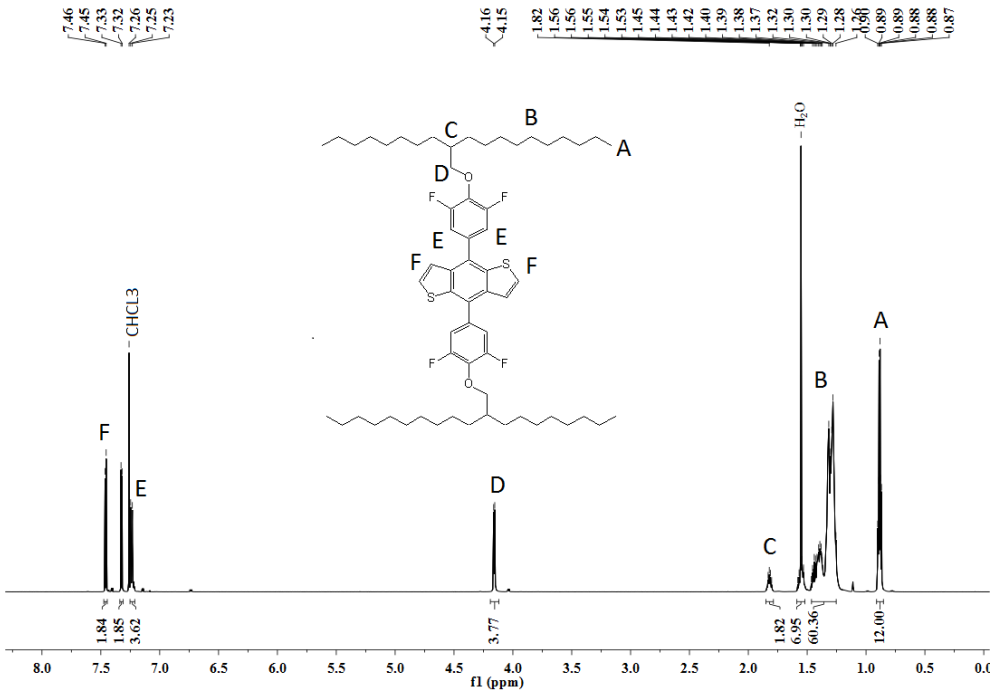

Figure A.4: H-NMR, 600 MHz.

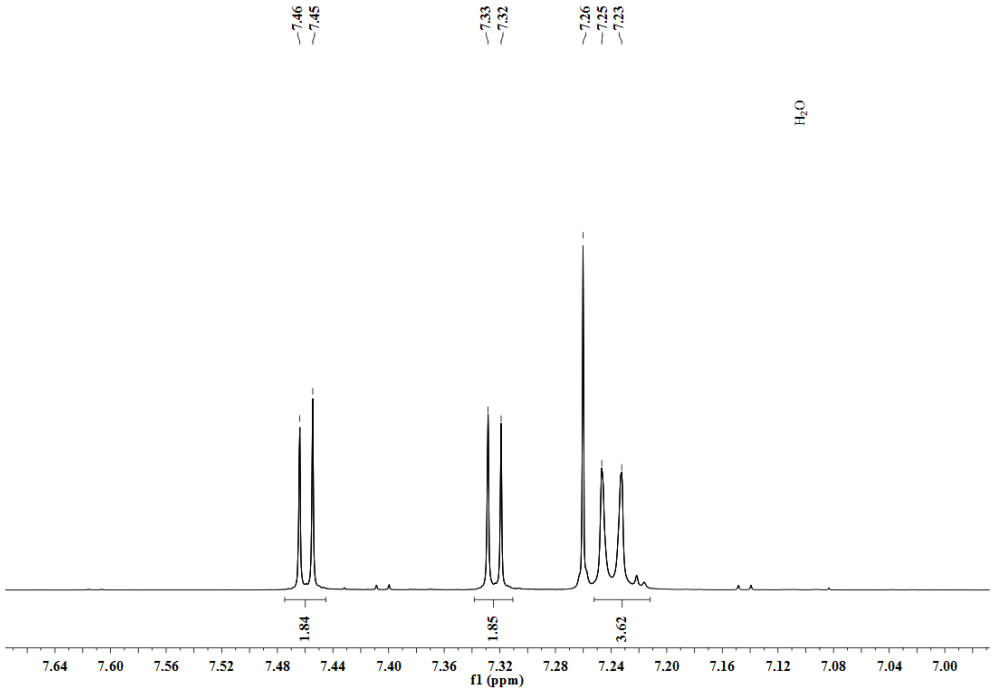

Figure A.5: H-NMR, 600 MHz.

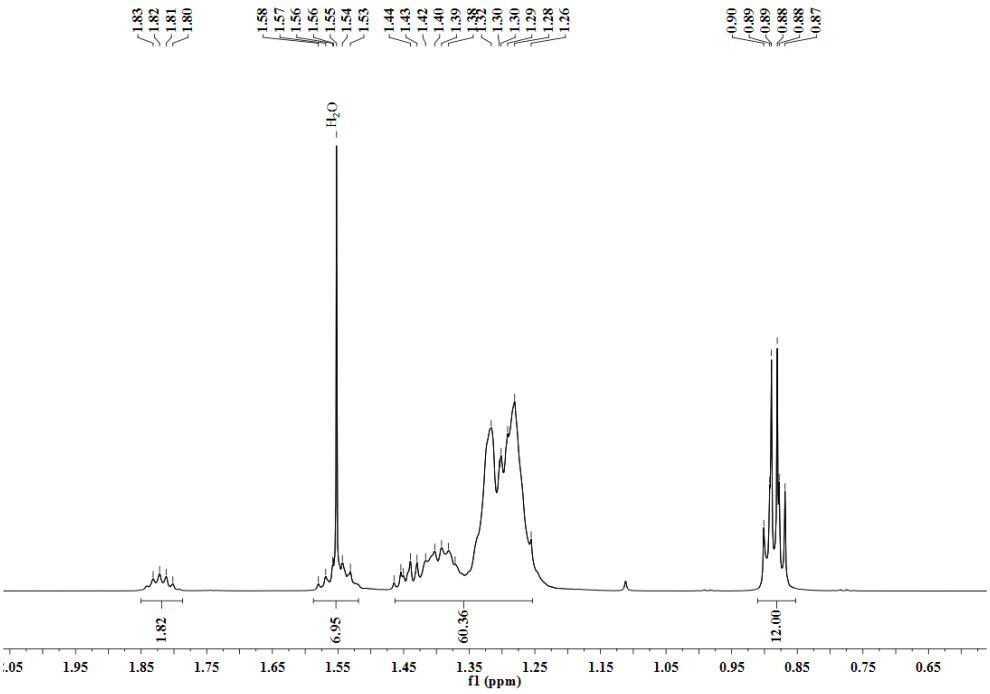

Figure A.6: H-NMR, 600 MHz.

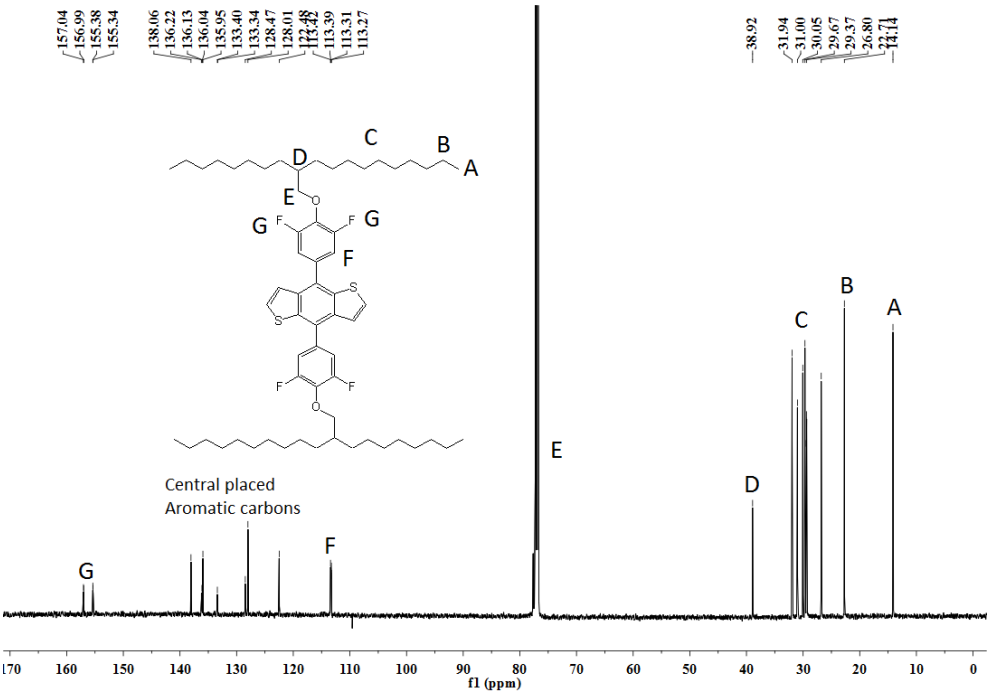

Figure A.7: C-NMR, 150 MHz.

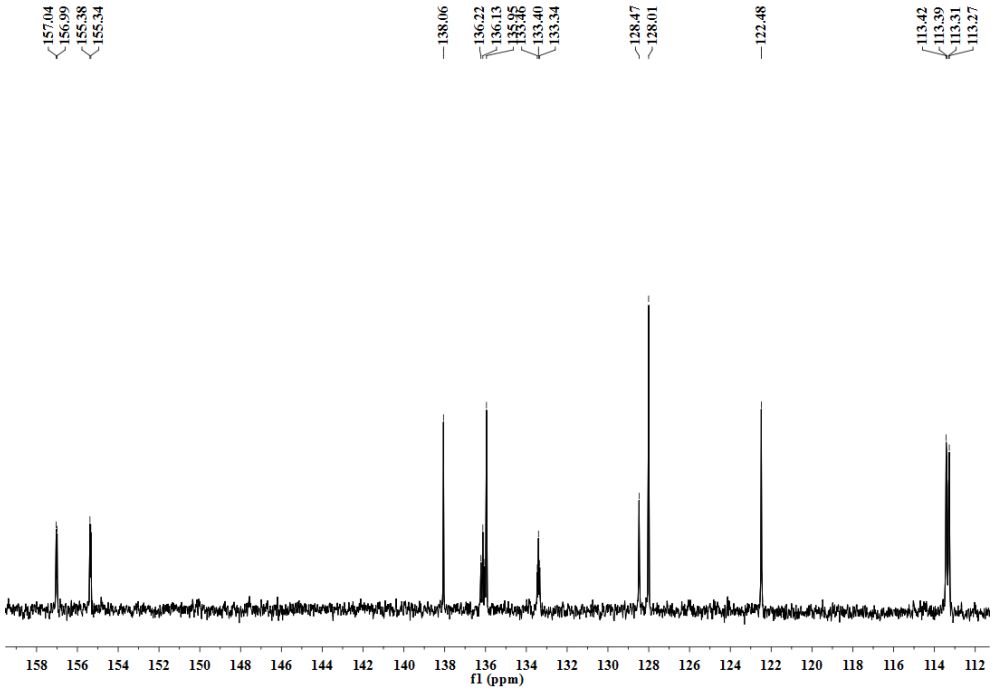

Figure A.8: C-NMR, 150 MHz.

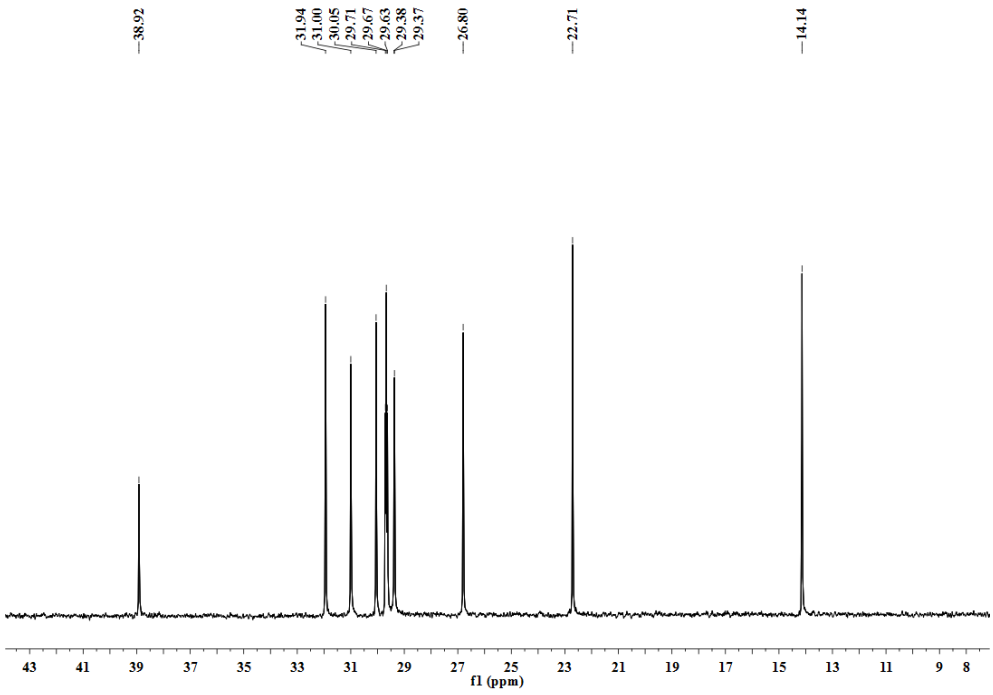

Figure A.9: C-NMR, 150 MHz.

A.4 NMR data for compound 4

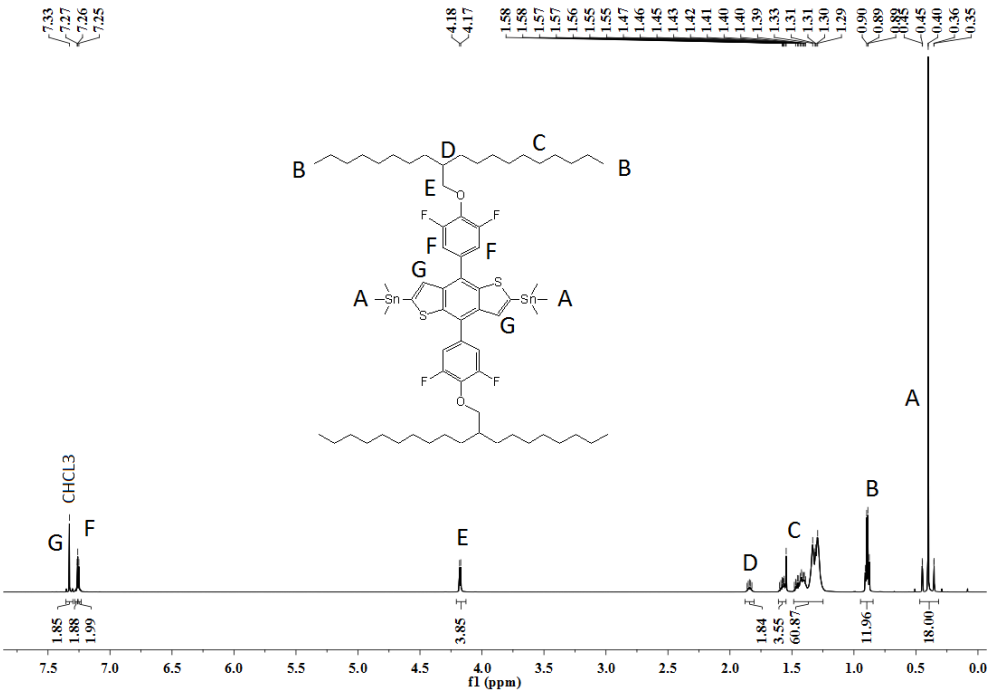

Figure A.10: H-NMR, 600 MHz.

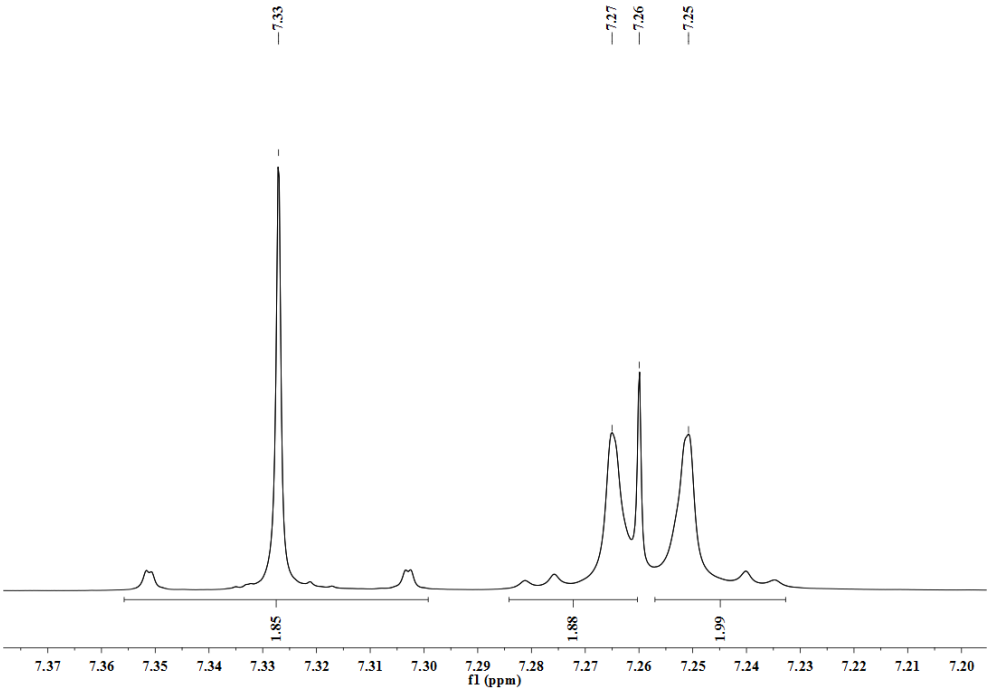

Figure A.11: H-NMR, 600 MHz.

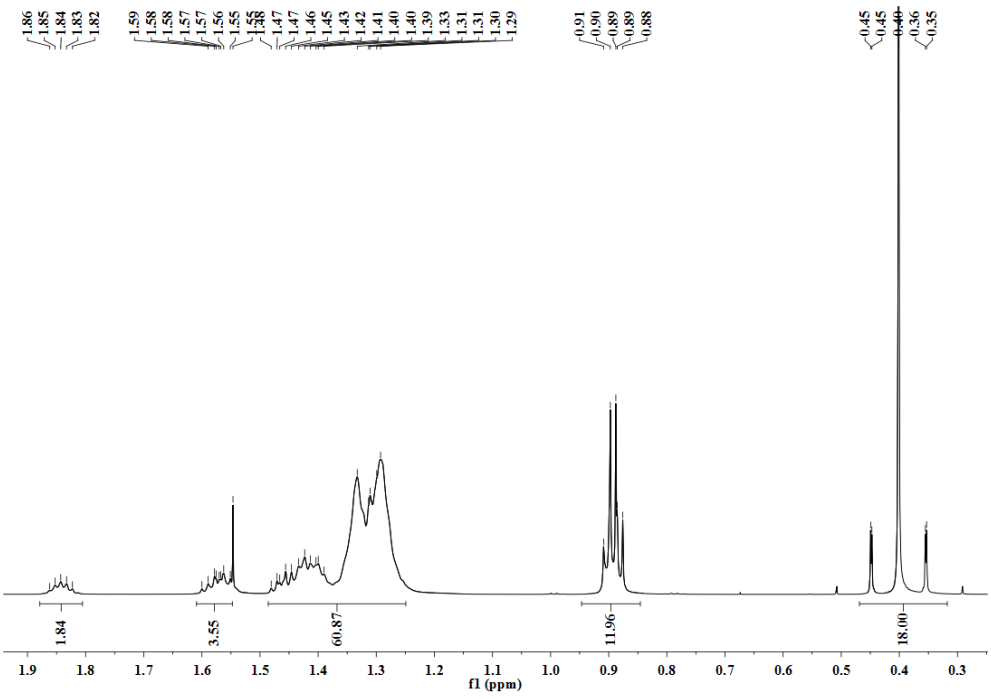

Figure A.12: H-NMR, 600 MHz.

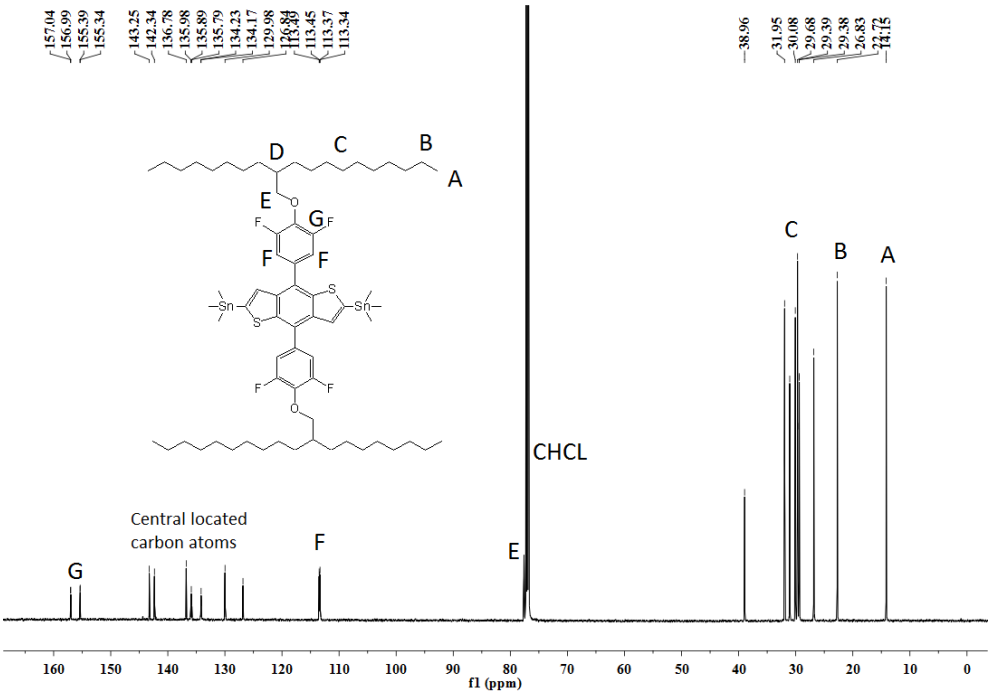

Figure A.13: C-NMR, 150 MHz.

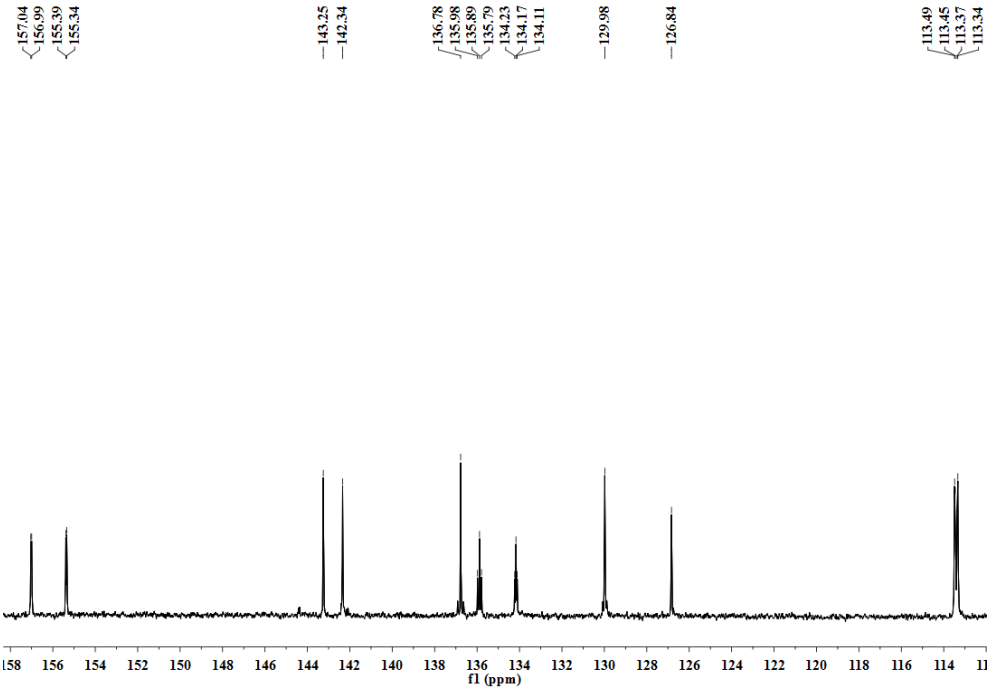

Figure A.14: C-NMR, 150 MHz.

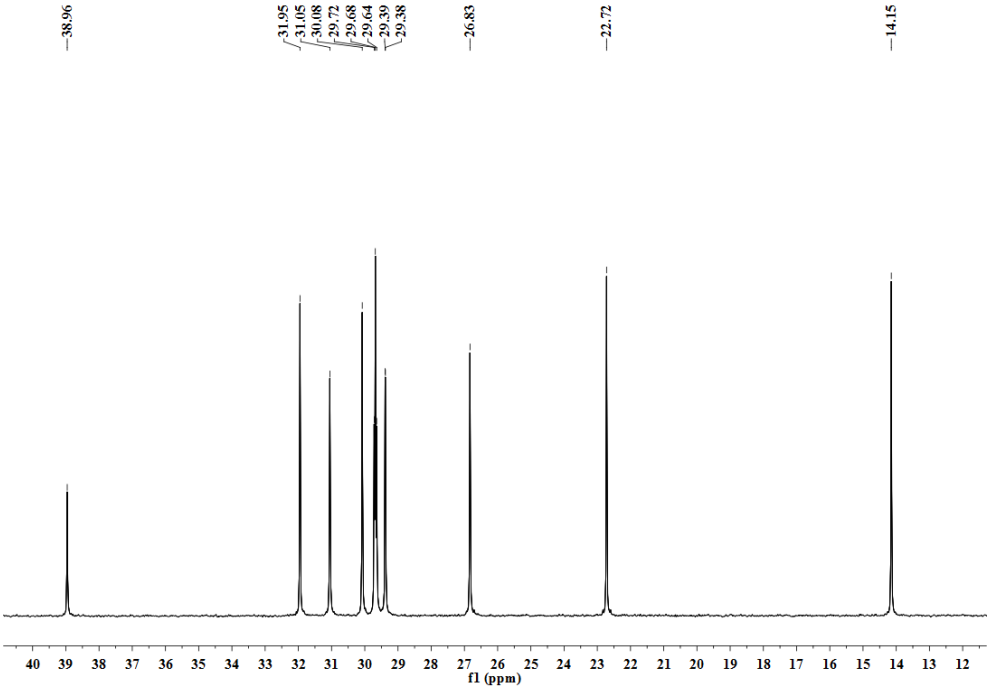

Figure A.15: C-NMR, 150 MHz.

A.5 NMR data for BDT-FS/TS-Sn

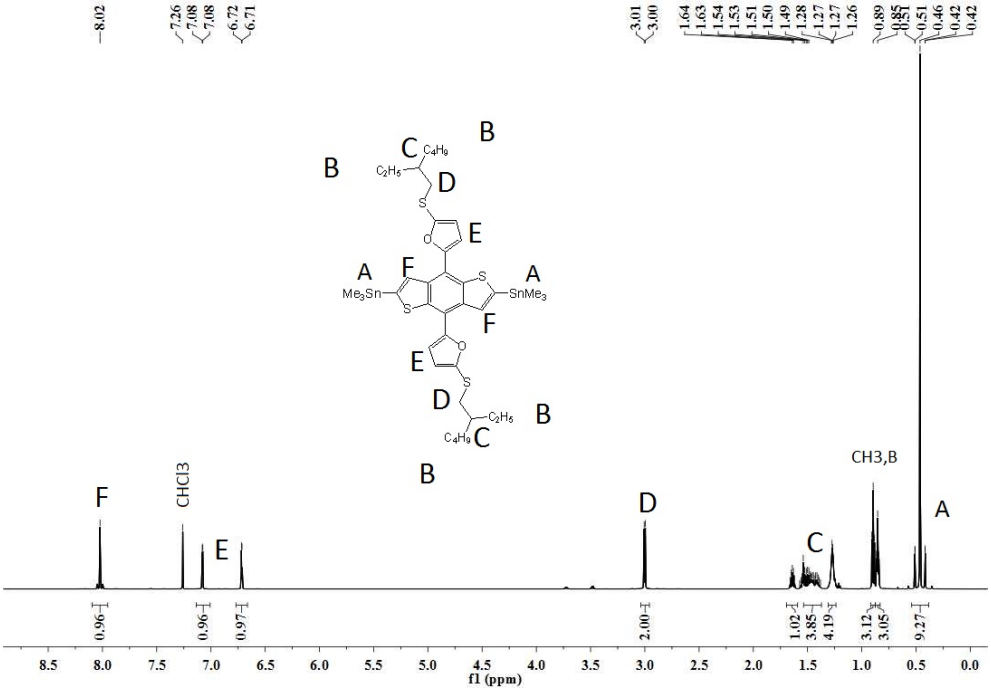

Figure A.16: H-NMR, 600 MHz. BDT-FS-Sn and BDT-TS-Sn

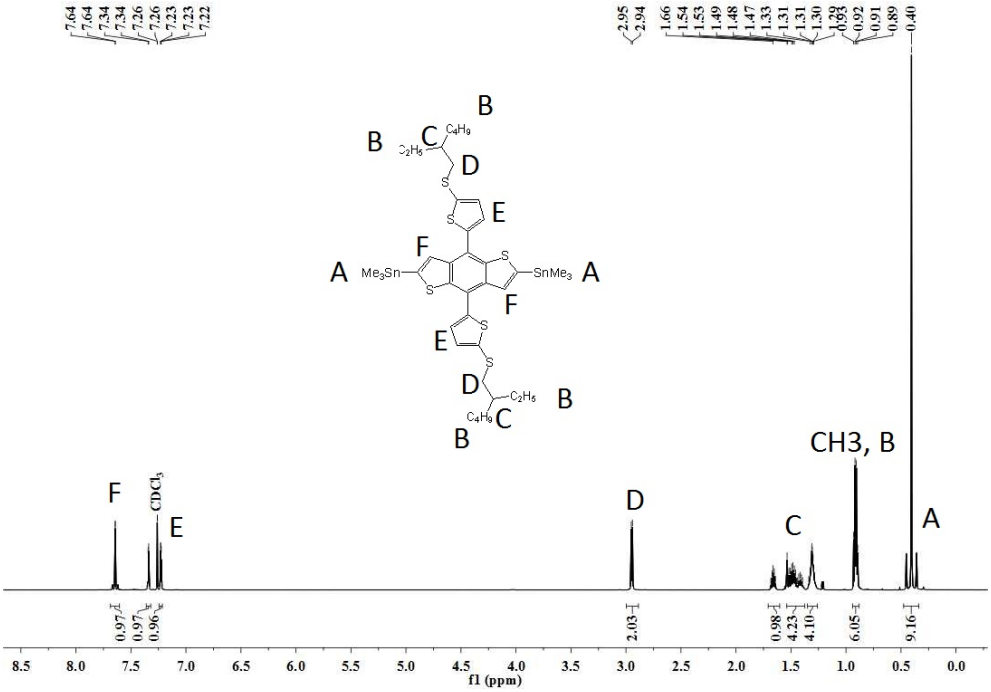

Figure A.17: H-NMR, 600 MHz. BDT-FS-Sn and BDT-TS-Sn

A.6 NMR data for DTBT, TPD and PTPD

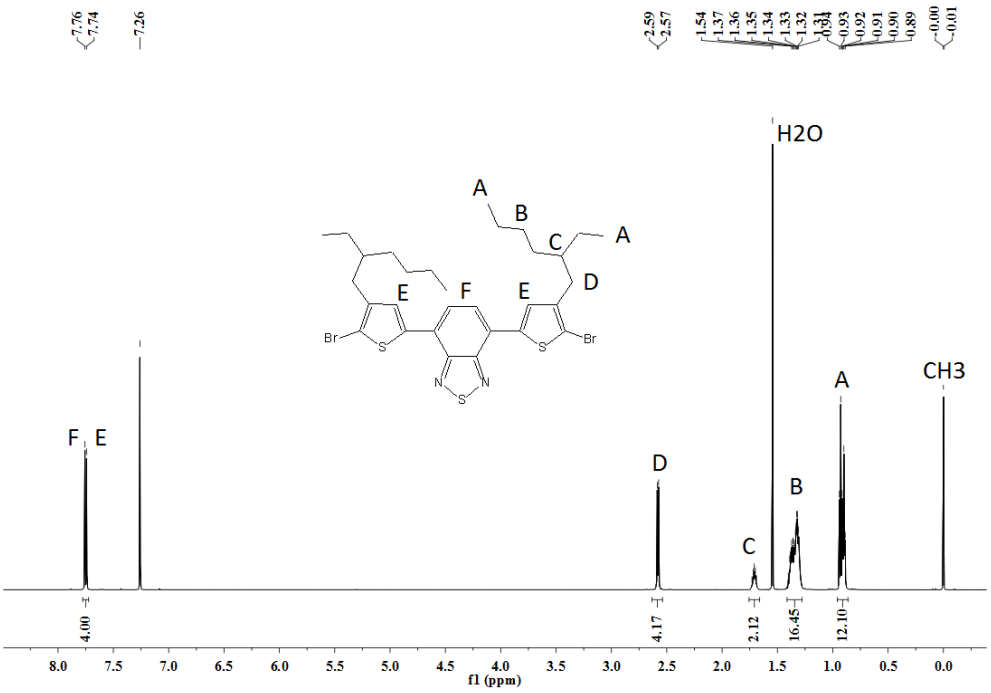

Figure A.18: H-NMR, 600 MHz. DTBT-br Acceptor.

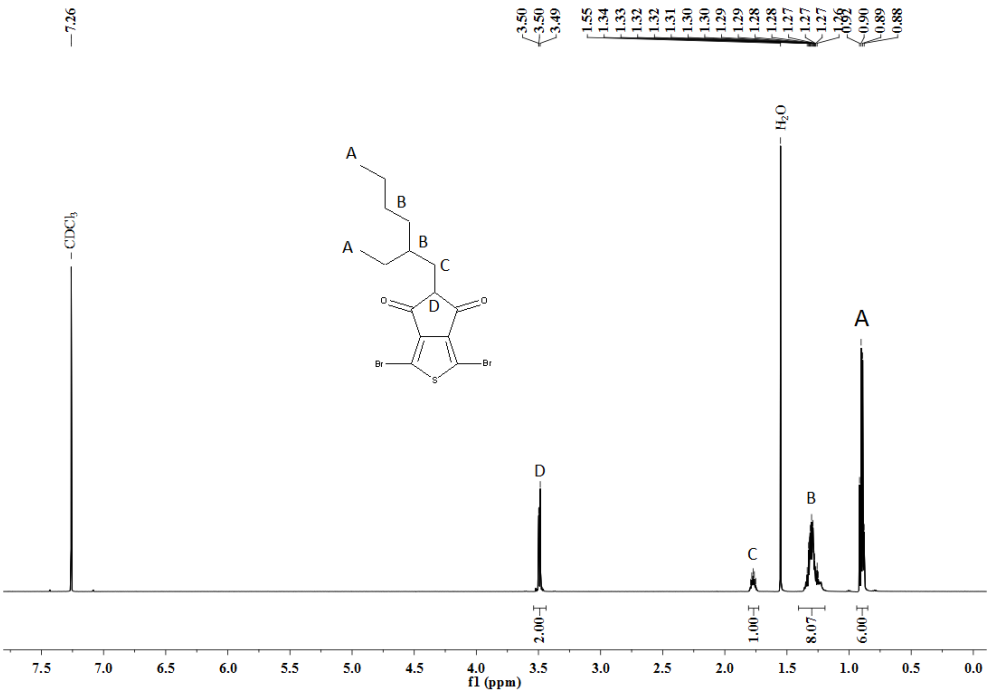

Figure A.19: H-NMR, 600 MHz. TPD-br Acceptor.

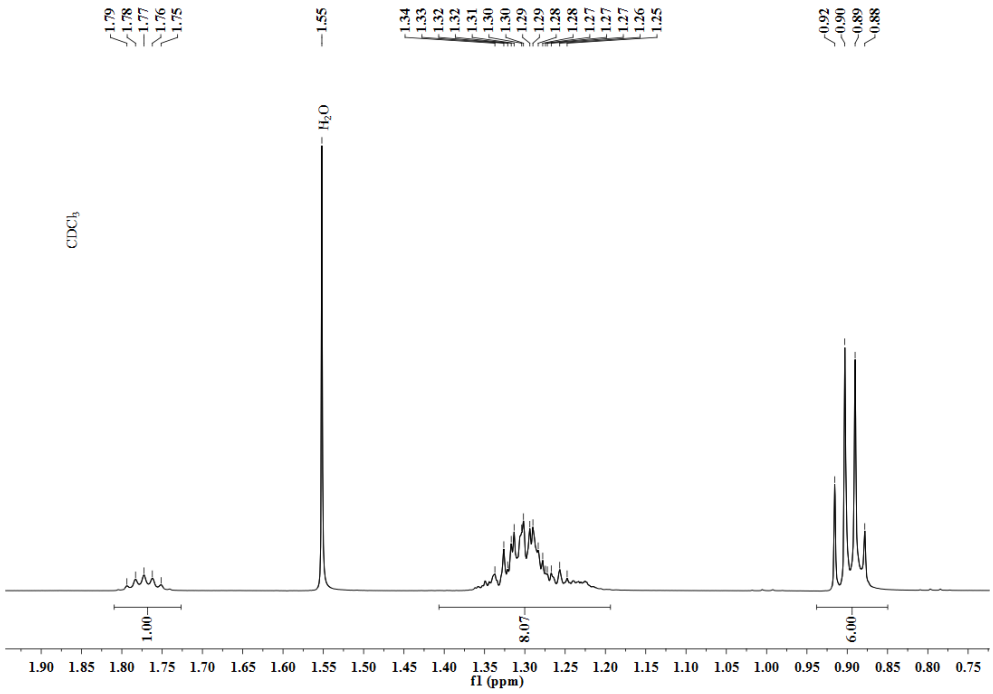

Figure A.20: H-NMR, 600 MHz. TPD-br Acceptor.

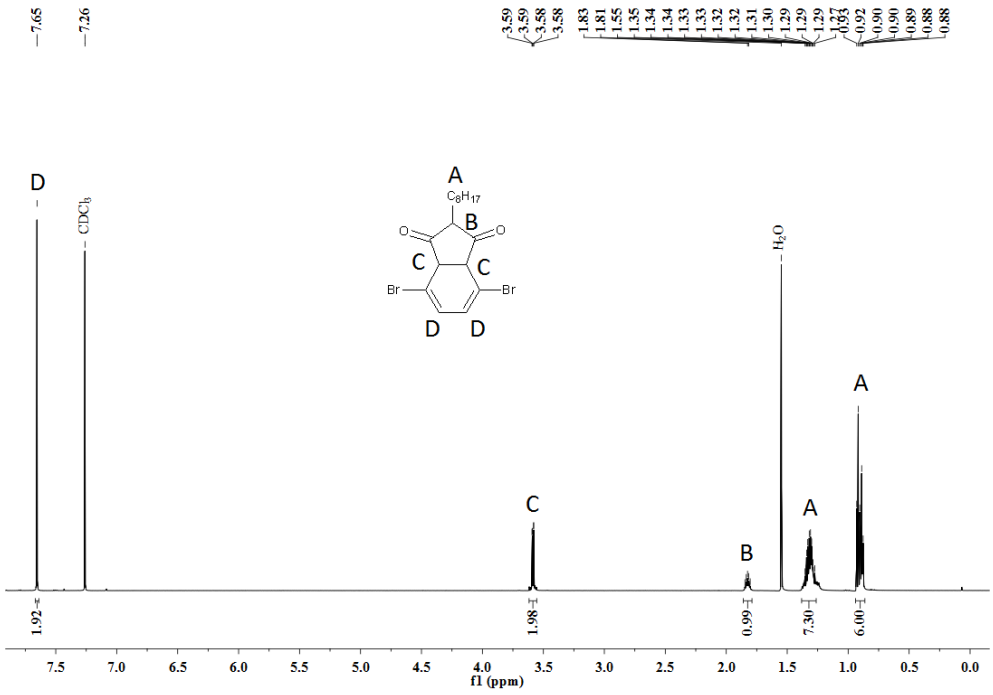

Figure A.21: H-NMR, 600 MHz. PTPD-br Acceptor.

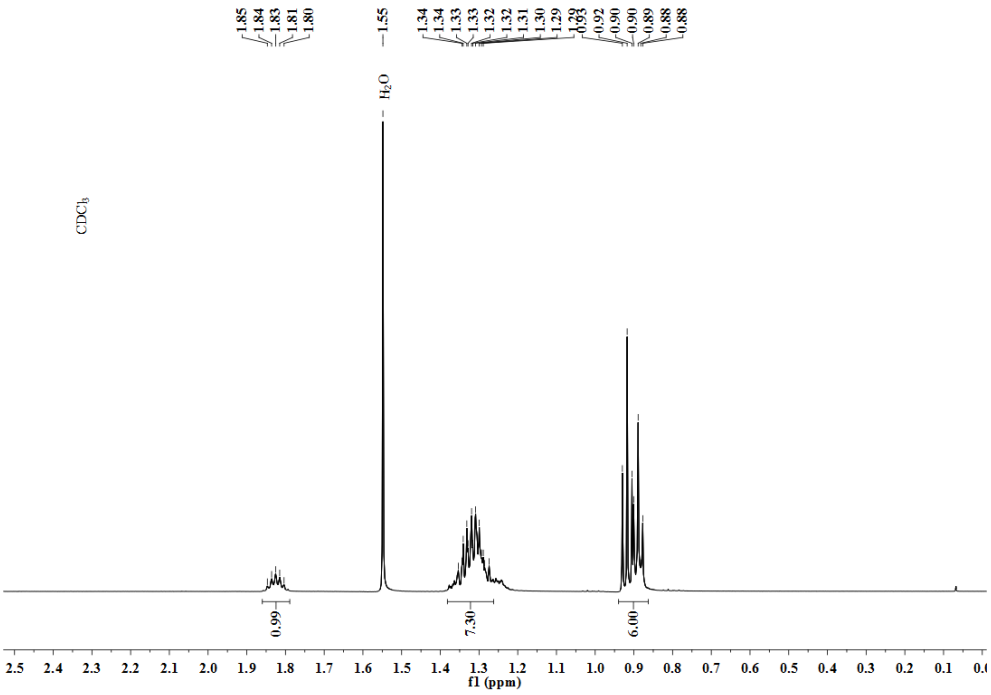

Figure A.22: H-NMR, 600 MHz. PTPD-br Acceptor.